Final report: Results of the shallow water marine habitat mapping with drones - MML 21817/08 05/2020 Sopimus vedenalaiskasvillisuuden kaukokartoitukseen soveltuvan menetelmän kehitystyöstä, Metsähallitus – FGI / MH 2166/2020.2

Authors: Lauri Markelin, Roope Näsi, Juha Suomalainen, Eija Honkavaara

Summary

Finnish Geospatial Research Institute (FGI) and Metsähallitus performed a joint campaign on 1st and 2nd September 2020 around the Vaasa area to map shallow water bottom habitats using hyperspectral drone remote sensing. Weather on both days was clear, sunny, and calm providing excellent conditions for campaigns. Metsähallitus chose three areas of interest and collected *in situ* vegetation samples, FGI performed two drone imaging flights on each area and did *in situ* reference measurements with three different spectrometers. Kaskinen (area size 3.5 ha) represented hard bottom type with sea floor elements larger than sand, i.e. sand, rocks, and stones. Huljan (area size 7 ha) and Haggisgrund (area size 3 ha) represented soft bottom types with sea floor elements smaller than sand, i.e. typically mud or clay.

FGI did all the data processing and analysis. One drone data set from each area was chosen for further processing and analysis. Images were orthorectified and hyperspectral image mosaics (maps) with 0.2 m ground sampling distance (GSD) and RGB mosaics with 0.015 m GSD were calculated. Image mosaic colors were converted to reflectance values by using reference reflectance panels installed on ground near the drone take off area. We measured average image reflectance values from each in situ location from circles of 0.8 m diameter. We tested three different segmentation methods (slic, quickshift and felzenszwalb from scikit-image python package) to find areas of homogenous vegetation from image mosaics. *In situ* spectrometry data was processed so that we got one averaged spectrum per sample from two sensors, ASD Field spec pro with wavelength range of 250-2500 nm, and SpecimIQ with wavelength range of 400-1000 nm. These *in situ* spectra were used to analyze spectral differences between samples, and after the spectra were integrated to match the bands of the hyperspectral camera used in drone, in comparison between image derived and *in situ* spectra of each sample. We used spectral angle mapper (SAM) algorithm to calculate similarities between different sample spectra.

The results showed that hyperspectral drone is suitable for mapping shallow water habitats. Successful mapping requires careful planning of the campaign, high quality calibrated sensors on board drone, and sophisticated analysis methods. We were able to create digital terrain models (DTM) of shallow sea bottom up to 1 meter depth, and digital surface models (DSM) describing the height of the sea floor habitats. We were able to create spectral angle maps showing potential areas for selected sample species. Segmentation of hyperspectral image mosaics can illustrate the potential vegetation areas of different species.

The resources reserved for this project were rather limited, and results obtained in this work are proof of concept regarding the potential of hyperspectral imaging in shallow water mapping with drones. There are several topics for further studies: the most important one would be to perform refraction correction for hyperspectral imagery to correct the effects of water transmittance at different wavelengths on sea bottom spectra. Secondly, more efforts should be used for getting meaningful and realistic segmentation of the image mosaics. Thirdly, more comprehensive and representative *in situ* reference measurements of each specimen should be done. Finally, to achieve more accurate results, the image classification should utilize not only spectral features, but combine spectral, textural and 3D features.

1. Introduction

This document is the final report of the project “Shallow water marine habitat mapping with drones” and completes the contract made between Finnish Geospatial Research Institute (FGI) and Metsähallitus in 2020. Work consisted of three work packages:

1. FGI Preliminary survey (delivered to Metsähallitus 28.8.2020)
2. Laboratory measurements (*In situ* reference measurements, performed 1.-2.9.2020)
3. Drone campaigns (performed 1.-2.9.2020 in Kaskinen and Vaasa area)

The results of packages 2 and 3 are described in this document.

This report is not written as a scientific article, but as freely formatted report. It describes the work done during the drone campaigns, data processing and analysis, gives results and discusses the findings, potential limitations, and gives recommendations for future work. References to previous work are given when possible.

1.1. Research questions

The general aim of the work was to see how hyperspectral drone-based remote sensing could be used to map shallow water (0 - 6 m) bottom habitats. The focus area was Baltic Sea, and especially vascular plants and algae. There were two different bottom types under interest: soft bottom (smaller than sand) and hard bottom areas. Metsähallitus provided a list of species under interest for both bottom types.

In the contract, Metsähallitus gave research questions that this research should try to give answers:

Research questions related to soft bottom habitats:

1. Can we define spectral differences between stoneworts (*Characea*, näkinpartaislevät) and vascular plants (mostly *Potamogeton/Stuckenia, Myriophyllum, Ranunculus*) -> defining their patch sizes automatically
2. Can we measure height of the vegetation?
3. Do *Potamogeton/Stuckenia* species differ from *Myriophyllum* species? What about Ranunculus species (have flowers on the sea surface)

Sheltered stonewort (Charophyta (Näkinpartaislevät)) bottoms listed as vulnerable (VU) in the Finnish red list of nature types, open stonewort bottoms as nearly threatened (NT).

Research questions related to emergent vegetation in soft bottoms:

1. Do sedges (sinikaisla, *Schoenoplectus tabernaemontani*) have different spectral features than reed (ruoko, *Phragmites australis*)
2. *Hippuris tetraphylla* versus other *Hippuris*, do they have spectral differences?

Research questions related to hard bottom habitats:

1. Width and depth of different algae zones. Possible heights of vegetation? Is it possible to get precise depth models?
2. Light changes with different depth, how does this effect spectral features?
3. Spectral differences between algae (green algae, brown algae, red algae), stonewort’s and vascular plants, mosses
4. Do epiphytic algae change the spectrum of *Fucus*? Could be used as status indicator for *Fucus* belts

Additionally, there was a research question related to work package 2, *in situ* measurements: analyze spectra of different species and see how they can be separated and classified.

Unfortunately, there were no *in situ* samples of *Ranunculus* species or any *Hippuris* species, so it was not possible to analyze spectra of these species. Also, we were not able to study research questions related to epiphytic algae and its effect on the spectrum of Fucus, as it would have needed a biologist to explain and show what epiphytic algae is. Finally, we were not able to analyze the effect of water depth to sample spectra due to limited resources.

2. Campaigns

2.1. Drone remote sensing system used

Data capture was carried out using a quadcopter drone, which was equipped with a multisensory remote sensing instrumentation. The main sensor was the FGI REHU (FGI Real-time Hyperspectral Camera and Processing Unit) sensor system for image acquisition (Figure 1, left). It consists of four separate sensors: two partly overlapping RGB cameras, visible range (VIS) and near-infrared range (NIR) snapshot hyperspectral cameras. VIS sensor collects 16 spectral bands between 450 nm and 650 nm and NIR sensor 25 spectral bands between 600 nm and 875 nm. Detailed properties of the FGI REHU are:

- RGB combined FOV: 91.8° x 35.0°
- VIS and NIR sensor FOV: 38.8° x 21.2°
- GSD at 100m altitude, RGB: ~4 cm, VIS: ~14 cm, NIR: 17 cm
- VIS sensor: 16 spectral bands between 450 nm and 650 nm
    - Approximate center wavelengths: 474, 484, 492, 507, 520, 534, 546, 569, 581, 594, 603, 617, 625, 637, 644, 648 nm
- NIR sensor: 25 spectral bands between 600 nm and 875 nm
    - Approximate center wavelengths: 657, 666, 673, 710, 735, 748, 760, 773, 838, 838, 848, 849, 861, 861, 863, 867 nm
- Spectral band widths (FWHM, full width half maximum) for VIS and NIR sensors are approximately between 15 nm and 30 nm
- The band widths and center wavelengths are just approximate descriptive values, as due to sensor characteristics, the spectral shape of each band varies significantly from the Gaussian shape

Additional instruments supporting FGI REHU were FGI AIRS (FGI Aerial Image Reference System, Suomalainen *et al.* 2018, Figure 1 right) which is collecting upwelling irradiance measurements and GPS timing info for FGI REHU, and Applanix15 GNSS IMU system for accurate position and orientation measurements. Furthermore, a small RGB camera GoPro HERO7 Black was installed to drone to collect photos during the data collection that could be used for visualization of the area of interest. See Figure 2 for the whole sensor setup used in the campaigns.

Figure 1. Left: FGI REHU, right: FGI AIRS.

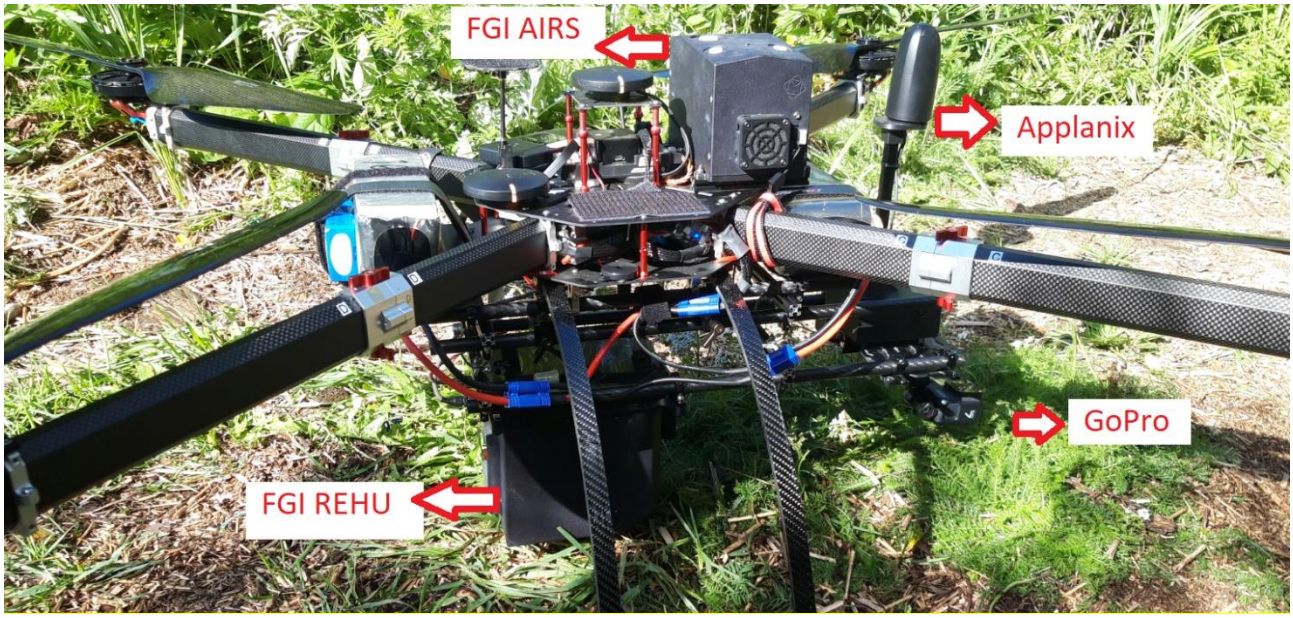

Figure 2. Drone remote sensing setup used during the campaigns.

2.2. Drone campaigns

Flight campaign took place on 1st and 2nd of September 2020 with blue sky and almost windless conditions, which was ideal weather for the measurements (Figure 3). Flights were performed in three areas namely, Kaskinen, Huljan and Haggisgrund (Figure 4). As visualization examples of each area, GoPro RGB drone images are given in Appendix 1. All three areas were flown twice, before and after the sample collection from the sea. Idea was that if the sample collection disturbs the sample areas and makes water turbid, the 1st flight data would be used for analysis and the second flight to match in situ sample locations from buoys installed by Metsähallitus crew. This was not possible for Kaskinen, as images taken on first flight were underexposed, and in Haggisgrund, where the area of first flight did not cover all the *in situ* locations. The flights were planned so that the areas can be covered during one flight taking 20 min and having 75% - 80% side overlaps between flight lines. Furthermore, azimuth angle (related to north) of flight lines was selected based

on solar azimuth angle (Figure 5). Due to different coverages of the areas different flying heights from 60 m to 100 m were used, causing GSDs of 10 - 17 cm for hyperspectral bands and about 1.5 - 4 cm for RGB cameras. Details of each flight are given in Table 1.

Three 1 m^2 sized reference reflectance panels were installed to the ground near the drone takeoff and landing area (Figure 6, left). These panels were used for reflectance calibration and additional quality reference for image data. Additionally, four geometric ground control points (GCPs) were installed around each water area, and their locations were measured with RTK GNSS system with centimeter accuracy (Figure 6, right). These GCPs were used to tie the images to the coordinate system during the geometric processing.

Table 1. Details of the drone flights. Bolded datasets were used for further analysis

Area	Date	Flight	Flight time (UTC +3)	Flying height (m)	Area (ha)
Kaskinen	1.9.2020	F1	10:03-10:27	75	3,5
Kaskinen	**1.9.2020**	**F2**	**11:00-11:20**	**75**	**3,5**
Huljan	**1.9.2020**	**F3**	**14:25-14:45**	**100**	**7**
Huljan	1.9.2020	F4	15:22-15:42	100	7
Haggisgrund	2.9.2020	F5	11:16-11:37	70	3,5
Haggisgrund	**2.9.2020**	**F6**	**12:50-13:10**	**60**	**3**

Figure 3. Clear blue sky and calm day at Kaskinen during the first campaign day.

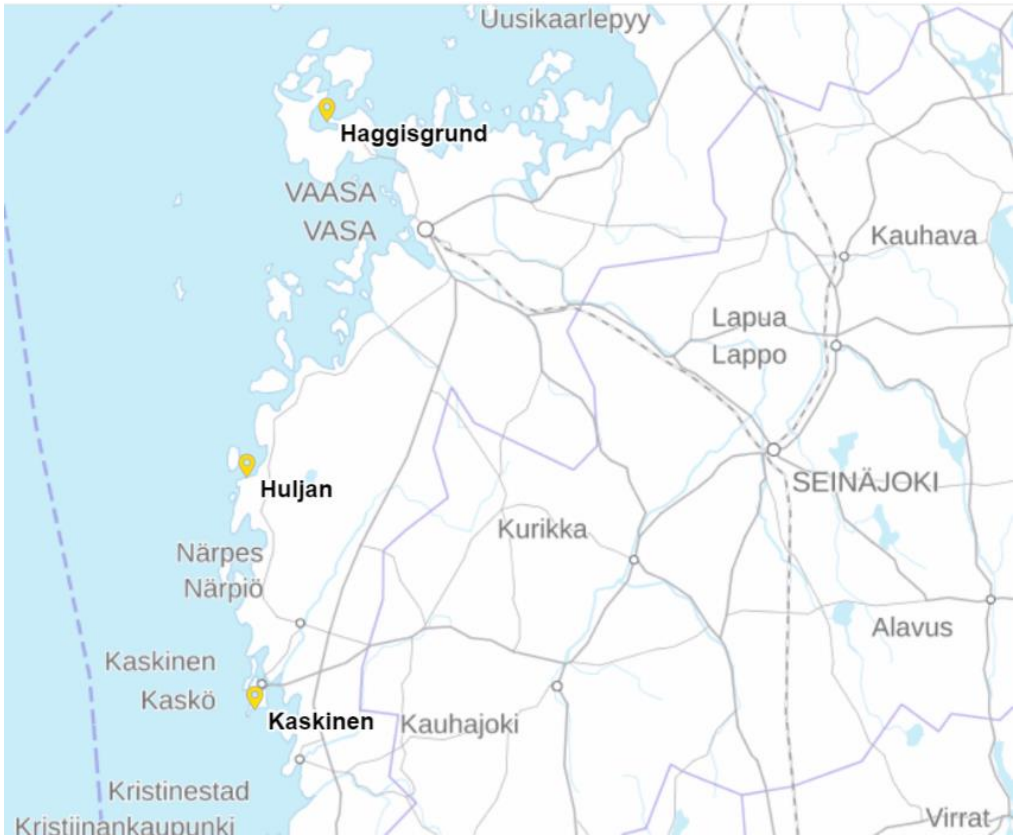

Figure 4. Location of the three study areas. Map from Paikkatietoikkuna.fi

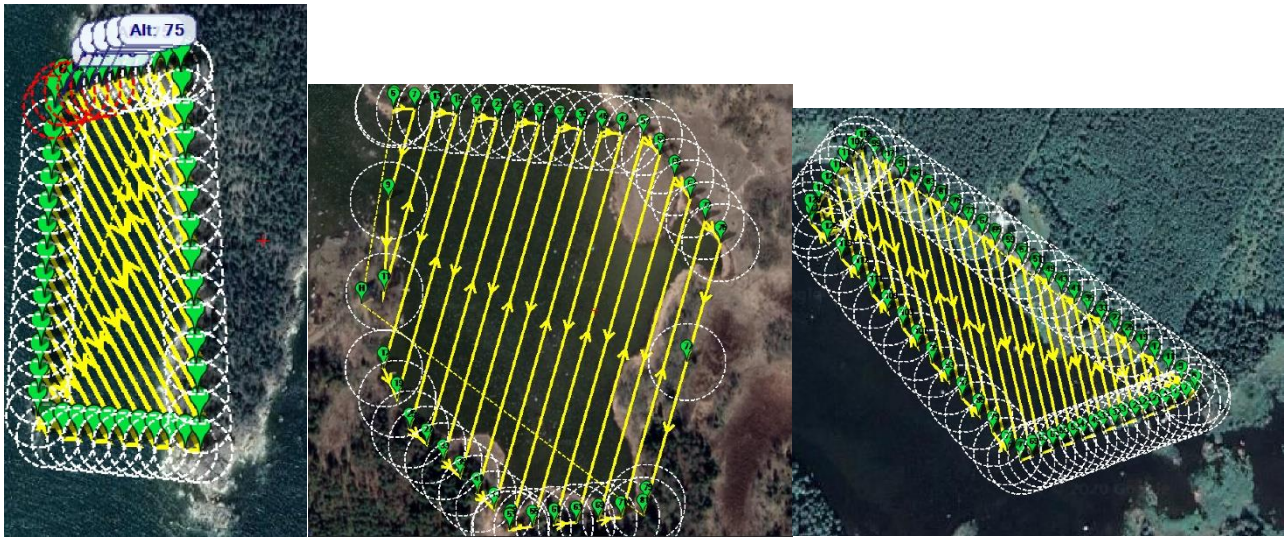

Figure 5. Drone flight lines for Kaskinen (left), Huljan (middle) and Haggisgrund (right).

Figure 6. Left: three reference reflectance panels at Kaskinen. Right: ground control point at Huljan.

2.3. *In situ* measurements

Metsähallitus crew collected *in situ* specimen samples from each three areas. Samples were named with codes and stored in plastic bags filled with water until they were measured at the end of both campaign days. At each in situ sample location, Metsähallitus crew measured the location with normal handheld GPS, water depth with Suunto diving watch, vegetation height and water temperature, and marked the location with orange buoy (Figure 7). GPS locations given in WGS84 system were later converted to ETRS-TM35FIN system using Paikkatietoikkuna.fi -service. Totally 24 individual samples were collected: 7 from Kaskinen, 9 from Huljan and 8 from Haggisgrund (Table 2). *In situ* sampling locations are shown in Figure 7 (right) Figure 8. In Kaskinen, two different samples of Fucus sp. (Hauru) were collected (sample names JP10 & P4). In Huljan, two different locations were marked for samples *Myriophyllum sp.* (ärviät, sample name JP28), *Potamogeton perfoliatus* (Ahvenvita, sample name T4) and *Callitriche hermafroditica* (Upposvesitähti, sample name A9). *Stuckenia pectinata* (Hapsivita, sample name S5) was found both from Huljan and Kaskinen. Details of the Metsähallitus *in situ* data are given in Appendix 2, and photos of all *in situ* samples are given in Appendix 3.

Table 2. List of all in situ samples marked on three campaign areas, their sample names, Latin names (Species) and Finnish names. In Kaskinen, two different samples of Fucus sp. were collected (JP10 and P4). In Huljan, samples JP28, T4 and A9 were marked on two locations (see Figure 8, left).

Kaskinen			Huljan			Haggisgrund		
Sample	**Species**	**Finnish name**	**Sample**	**Species**	**Finnish name**	**Sample**	**Species**	**Finnish name**
PE13	Fontinalis sp.	Näkinsammal	JP28	Myriophyllum sp.	Ärviät	A1	Chara aspera	Mukulanäkinparta
JP10	Fucus sp.	Hauru	S5	Stuckenia pectinata	Hapsivita	M10	Zannichellia sp.	Haurat
K2	Furcellaria lumbricalis	Haarukkalevä	T4	Potamogeton perfoliatus	Ahvenvita	A1	Chara aspera	Mukulanäkinparta
P4	Fucus sp.	Hauru	T4	Potamogeton perfoliatus	Ahvenvita	S5	Stuckenia pectinata	Hapsivita
LV4	Stuckenia pectinata	Hapsivita	A9	Callitriche hermafroditica	Uposvesitähti	MA2	Chara tomentosa	Punanäkinparta
JP07	Rhodophyta	Punalevät	A9	Callitriche hermafroditica	Uposvesitähti	LV2	Phragmites australis	Järviruoko
6	Chlorophyta (Ulva sp.)	Viherlevät, tn. suolilevät	M4	Najas marina	Merinäkinruoho	KE3	Schoenoplectus tabernaemontani	Sinikaisla
			JP28	Myriophyllum sp.	Ärviät	AKI1	Lemna trisulca	Ristilimaska
			M4	Najas marina	Merinäkinruoho			

Figure 7. Left: buoys used for marking in situ sampling locations. Right: Kaskinen in situ sampling locations.

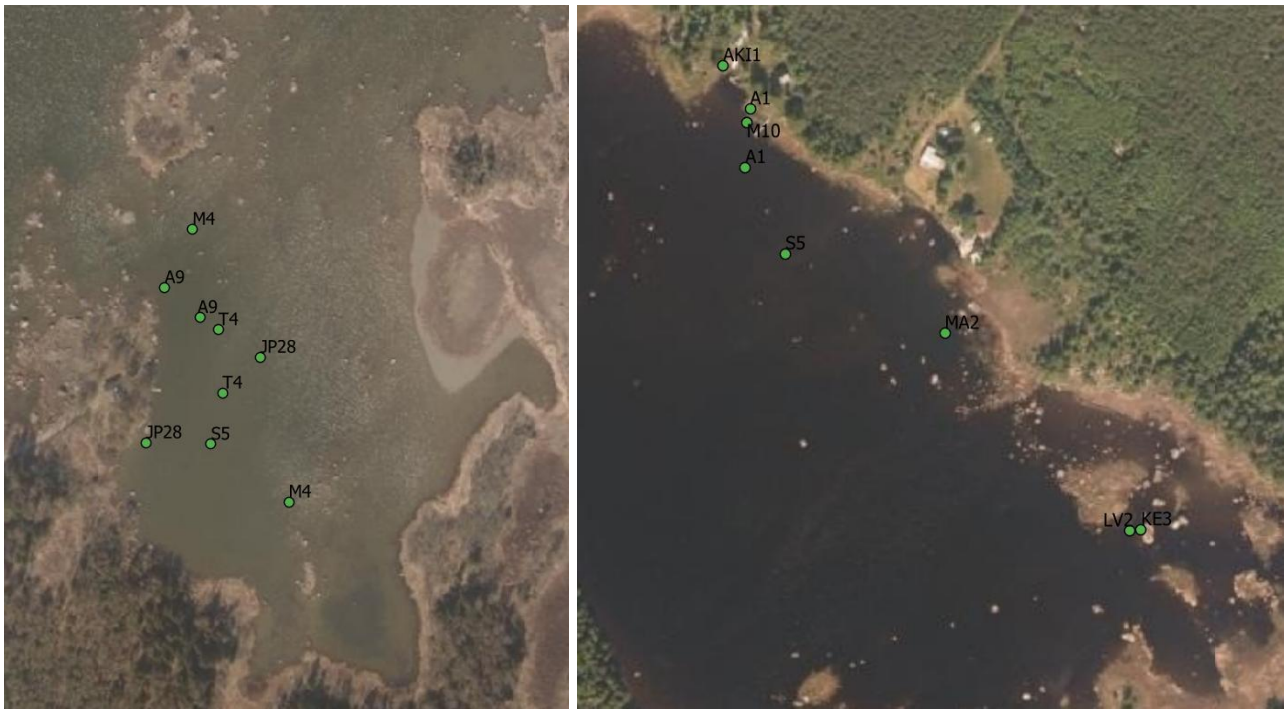

Figure 8. In situ sampling locations for Huljan (left) and Haggisgrund (right).

Specimen samples provided by Metsähallitus were measured in the ground just after the drone flights. Samples were measured with two instruments: 1) The ASD Field Spec Pro point spectrometer (ASD, Analytical Spectral Devices, Boulder, CO, USA, Figure 9), with 350 - 2500 nm spectral range; 2) The SpecimIQ (Specim Ltd, Oulu, Finland) hyperspectral camera having a spectral range from 400 to 1000 nm (Figure 9).

Spectralon white reference panel was used to calibrate ASD spectra to reflectance values. Five individual spectra were measured from each sample, and Spectralon was measured before and after each sample. Separate small white reference panel was installed next to samples and used for calibrating SpecimIQ images to reflectance values (Figure 10).

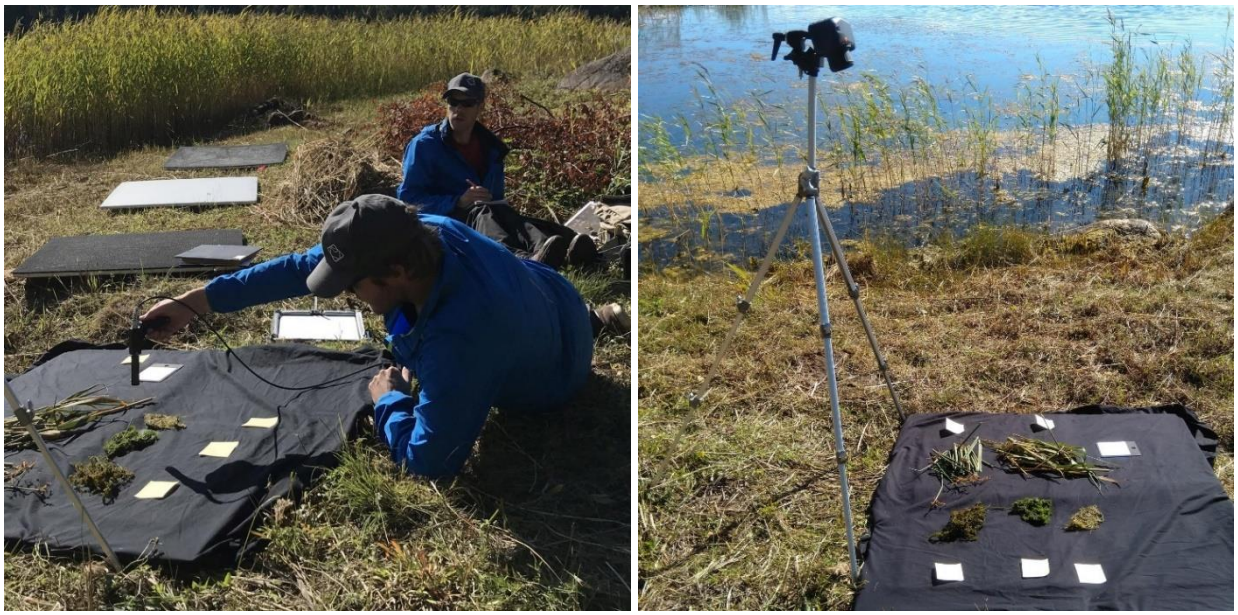

Figure 9. Left: in situ reflectance measurements with ASD point spectrometer (photo by Essi Keskinen). Right: in situ reflectance measurements with SpecimIQ hyperspectral camera.

Figure 10. Example photo of three in situ samples and small white reference panel for SpecimIQ.

3. Methods

3.1. Drone data preprocessing

3.1.1. Geometric and photogrammetric processing

To preprocess the raw data, the REHU raw RGB images were converted to TIFF format and an RGB composite image was generated from each REHU hyperspectral image. The AIRS post-processing software was used to calculate a Post-Processed Kinematic (PPK) position for each REHU image.

These data were then processed in Agisoft Metashape software (version 1.6.2). The RGB and RGB-composite images were loaded to Metashape with the AIRS GNSS positionings. The coordinates of the GCPs were also loaded in and each GCP was pointed on at least 10 RGB images. Next, the RGB and RGB-composite images were photogrammetrically aligned together using the Metashape Align tool in “High”-accuracy setting. As typically some of the images failed to align correctly, the misaligned images were attempted to realign to the correctly aligned images using “Highest”-setting. Finally, the all still misaligned images and clearly false tie points were removed, and the alignment was optimized. At this point, the external image orientations of the hyperspectral images and the and camera lens calibration parameters of the hyperspectral cameras were exported to be used in the radBA processing step. The hyperspectral images were then disabled in the Metashape processing as they were no longer used in further processing steps.

Next, the work in Metashape was continued to produce the 3D model of the area. The “Dense point cloud tools” was used to generate a dense point cloud from the RGB images using “High quality”-setting and with calculation of point confidences enabled. The unreliable parts of the dense point cloud were then filtered and cropped using the point confidence parameter. The on-land areas, except 1-2 meters next to the shoreline, were manually removed from the data. The dense cloud Detect Ground Points-tool was then used (Max angle=5.0°, Max Distance = 0.05 m, Cell Size = 10 m) to detect water bottom below the underwater vegetation. Then two digital surface models were generated and exported in GeoTIFF format. The Digital Terrain Model (DTM) was generated using only “ground” points and this followed the water bottom below the underwater vegetation. The Digital Surface Model (DSM) was generated using all points and this described the top of the underwater vegetation. Finally, the RGB images were projected on the DSM and an RGB orthomosaic calculated and exported in GeoTIFF format. Ground sampling distances of RGB image mosaics, DTMs and DSMs were processed to 15 mm or 0.015 m.

3.1.2. Radiometric processing and hyperspectral image mosaic calculation

To convert the REHU hyperspectral pixel data values to reflectance factors, first, the raw REHU hyperspectral data cubes were converted to radiance data cubes. On each flight, one data cube with good central view of the reference reflectance panels was located and the panel radiances were sampled from the center pixels of the two panels. Finally, a two-point empirical line method was used to determine transformation parameters for the radiance-to-reflectance factor conversion (Smith and Milton, 1999).

Then the hyperspectral orthophoto mosaics were calculated from the radiance data cubes using the FGI’s radBA software (Honkavaara and Khoramshahi, 2018) utilizing the Metashape internal camera parameters and image exterior orientations, Metashape DSM, and the reflectance transformation parameters. On average, the hyperspectral image block had 80% overlap along path and 75% cross path, giving approximately 10 image views to each object location. We evaluated two approaches to calculate the mosaics from the overlapping images. Firstly, we used the so called most-nadir method, where those parts were used from the images that were the closest to the vertical view. However, the different views to the object resulted in nonuniform reflectance over the water areas. Secondly, we used a median filtering -based approach, i.e. the median reflectance value was selected from the overlapping images to the mosaic. The median filtering -approach removed visible image borders and reduced some noise from mosaics, providing good quality hyperspectral reflectance mosaics.

Median filtered mosaics were selected for the further evaluations. Examples of the mosaics produced using the most-nadir and median filtering methods are shown in Figure 11. Final ground sampling distances of each hyperspectral image mosaics were 20 cm or 0.2 m.

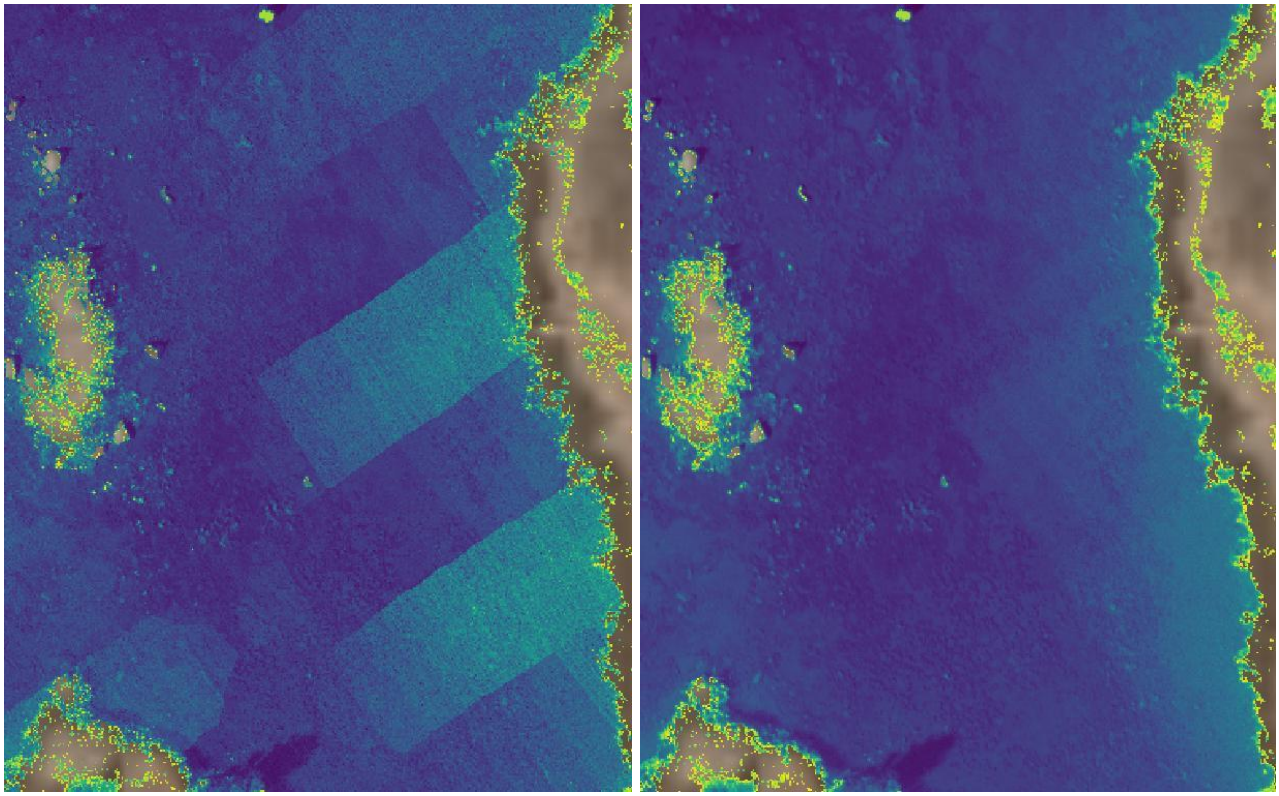

Figure 11. RadBA image mosaic processing results using most-nadir (left) and median (right) methods. Image borders from adjacent flight lines and some noise is clearly visible in most-nadir version (left). Detail from Huljan area.

3.2. *In situ* data processing

Five ASD spectra from each sample were averaged to get one ASD reference spectra per sample. As ASD is a point spectrometer and sample sizes were relatively small, it is possible that some of the sample spectra may include small proportions of the black background fabric. Examples of ASD spectra are given in Figure 12. SpecimIQ camera provided automatically calibrated reflectance image of the area of interest (Figure 13). Five pixel locations from each sample were marked, and an average of 3x3 pixel area was calculated to get five different spectra per sample (Figure 14, left). The pixel locations were chosen to be as representative of the sample structure as possible, including points from leaves and stem depending on the sample. Then, the five SpecimIQ spectra from each sample were averaged to get one SpecimIQ spectra per sample. Additionally, standard deviation of five spectra per band were calculated. These standard deviations are shown in individual spectra plots as +-confidence intervals. Finally, SpecimIQ reference spectra were integrated to FGI REHU spectral responses to make quantitative image – reference comparison possible (Figure 14, right).

In the final analysis with image derived spectra, only SpecimIQ -data was used as reference. This was because with SpecimIQ data we could be sure that the sample spectra did not contain any disturbances from the background.

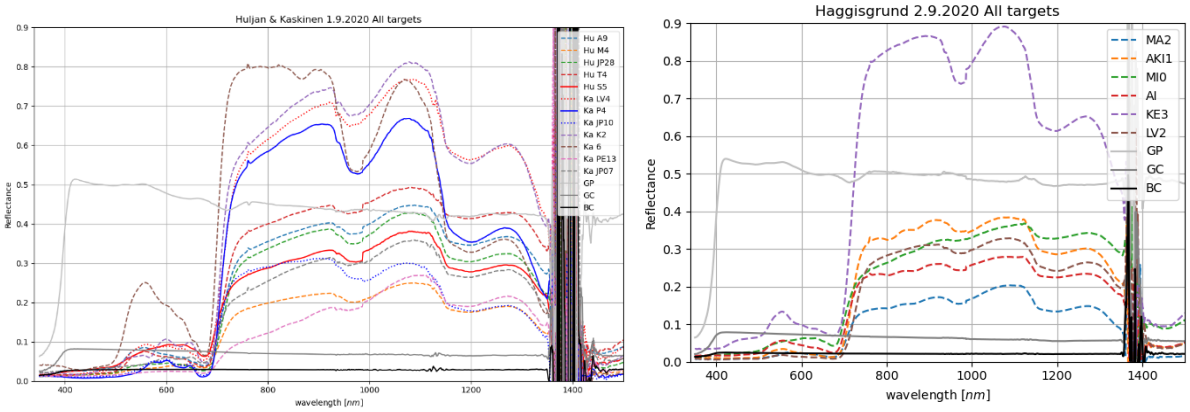

Figure 12. ASD sample spectra measured on 1st (left) and 2nd September (right). BC, GC and GP are three reference reflectance panels. Disturbances in spectra around 1400 nm are due to atmospheric water absorption and can not be avoided in spectral measurement done outside in natural light.

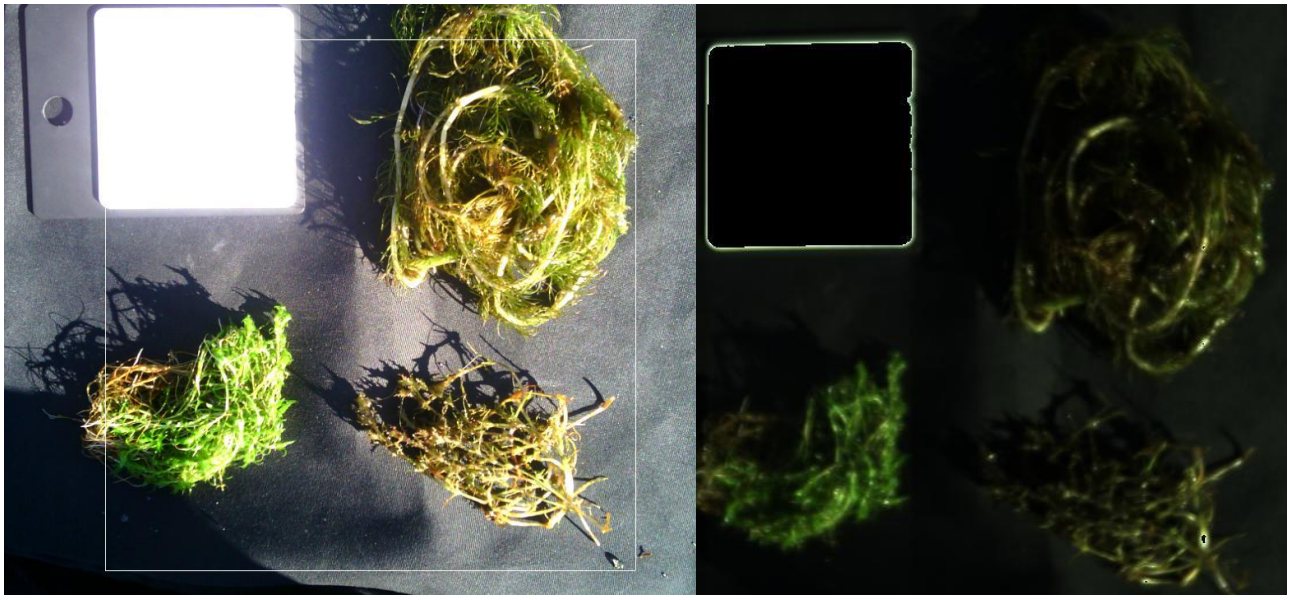

Figure 13. Left: SpecimIQ viewfinder image of the samples. Right: SpecimIQ reflectance image (RGB composite) where the white reference panel is automatically detected.

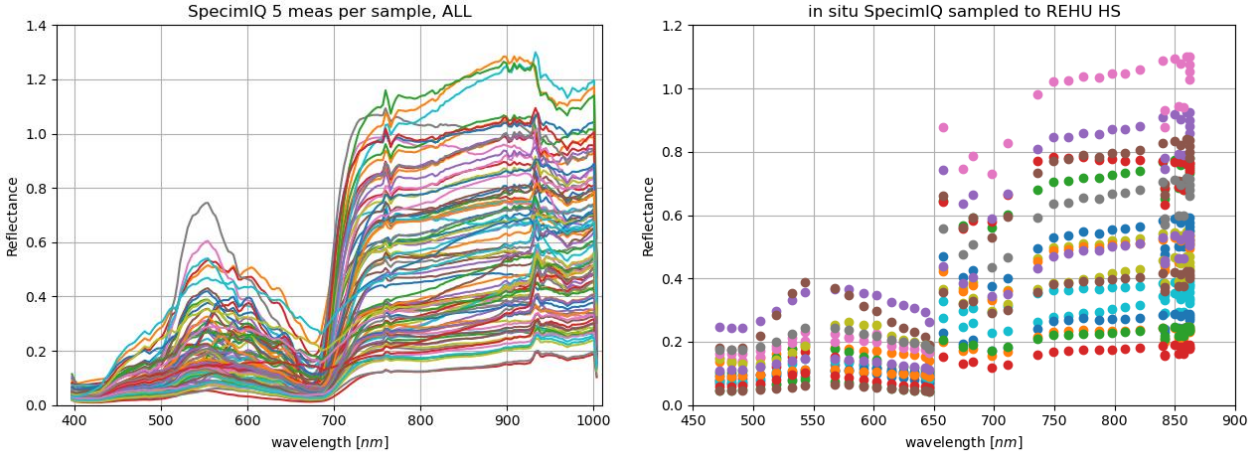

Figure 14. Left: all SpecimIQ in situ sample spectra (five per sample). Right: SpecimIQ spectra sampled to FGI REHU bands (one averaged spectrum per sample).

3.3. Data analysis

3.3.1. General

To find answers to given research questions, three different type of data analysis were made: first, *in situ* spectra of samples were compared both visually and quantitatively to see potential spectral differences or similarities between samples. Secondly, *in situ* reference spectra were compared to image spectra measurements from *in situ* locations to see how well image spectra matches with reference data. Finally, attempt to segment, classify, and map whole image area was done to find distribution and potential areas of reference sample species.

In addition to visual comparison of different spectra, two algorithms were used to estimate similarities of the spectra. Spectral Angle Mapper (SAM) and Chi-square (X^2) metrics were used to evaluate the similarities in spectral shapes (Kruse *et al*. 1993, Markelin *et al*. 2017).

The spectral angle is a metric comparing spectral shapes, insensitive to spectral amplitude, and is calculated as:

$$\alpha = \cos^{-1}\left(\frac{\sum_{i=1}^{nb} a_i t_i}{\sqrt{\sum_{i=1}^{nb} a_i^2}\sqrt{\sum_{i=1}^{nb} t_i^2}}\right), \quad (1)$$

where *a* denotes image spectra, *t* are reference spectra and *nb* is the number of channels/bands in a spectrum. In practice, the spectral angle is the angle between two vectors (spectra) and is not sensitive to differences in amplitude that are consistent over the whole spectrum. The range for the spectral angle is [0, 180] (or 0–π radians), where values close to 0 indicate high similarity.

Chi-square takes both the shape and the amplitude of the spectra into account, where the sum of all bands is considered for each spectrum, and is calculated as:

$$X^2 = \sum_{i=1}^{nb}\left(\frac{(a_i - t_i)^2}{t_i}\right), \quad (2)$$

where *a*, *t* and *nb* are as in equation (1). Chi-square values close to 0 indicate high similarity.

SAM was used in all spectral analysis; Chi-square was used only when comparing sample spectra between *in situ* reference data. Additionally, modified version of spectral angle mapper, msam, was used in the comparison of *in situ* and image derived spectra from *in situ* locations. In msam, both spectra under comparison are mean subtracted prior to spectral angle calculation. Results are normalized such that the maximum value of 1 corresponds to a perfect match (zero spectral angle) (SpectralPython, 2021).

3.3.2. Image derived spectra analysis

When analyzing hyperspectral image mosaics, only REHU VIS-sensor 16 bands were used. This was because most of the reflectance spectra values of REHU NIR bands were negative, and their shapes did not match with the REHU VIS bands i.e. image spectra created with REHU VIS + NIR had clear discontinuity between sensors. Potential reasons for this are discussed in section 4.

From each in situ location, average reflectance over area of 0.8 m diameter circle was calculated from the hyperspectral image mosaics. The average reflectance were extracted using the algorithms developed in Nevalainen *et al.* (2017) and modified to be suitable for water targets.

In this work, we performed simple supervised classification for each image pixel with Spectral Angle Mapper. In SAM, spectra of each pixel is compared to all reference spectra (7 for hard bottom (Kaskinen), 11 for soft bottom (Huljan and Haggisgrund)), and pixel is classified to class with smallest spectral angle. Additionally, we created spectral angle maps of selected individual species as an attempt to map the most potential areas of that specimen.

We also tested three different segmentation algorithms to see if we could find areas of different species. Algorithms used, slic, quickshift and felzenszwalb were from scikit-image python package (version 0.18.3, Skimage 2021). Before segmentation, simple mask was created to mask out land and leave only water areas for analysis. Masks were created by thresholding pixels of one REHU NIR band. Idea was that land vegetation has much stronger reflectance values in the NIR spectral range compared to water. After thresholding, small holes inside water area were connected to mask, and some large remaining areas on land were removed. Each segmentation algorithm had several parameters, and some experiments and iterative runs were made to find suitable values for each parameter. After segmentation, segment average reflectance spectra were calculated using the same modified Nevalainen *et al.* (2017) method as for *in situ* locations. Unfortunately, due to limited time, classification of segmented images was not done.

4. Results and discussion

4.1. *R*esults based on analysis of *in situ* spectra

4.1.1. General results

Analysis of the SpecimIQ reflectance spectra of the *in situ* samples showed that some samples have relatively large within sample deviations in spectra i.e. sample spectra varies depending on the specific measurement location on sample. This was expected behavior, as individual spectrum can be measured from different parts of specimen, and there are variations in illumination, bright and shadowed spots in the sample. Example SpecimIQ spectra of two samples and photos of those samples are given in Figure 16, and photos of these samples in Figure 16. All SpecimIQ spectra are given in Appendix 4.

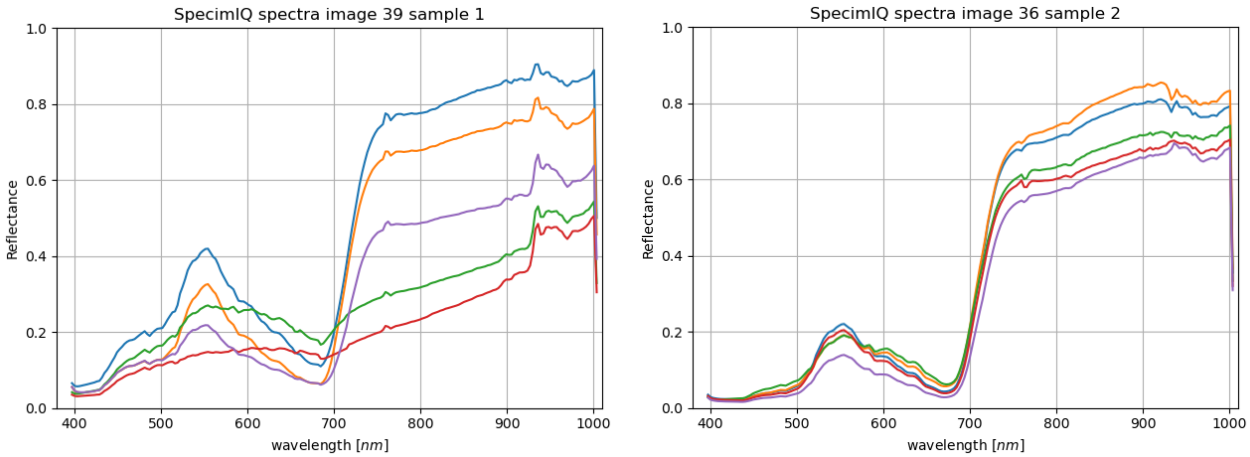

Figure 15. 5 SpecimIQ spectra of samples KE3 (Schoenoplectus tabernaemontani, left) and LV4 (Stuckenia pectinata, right).

Figure 16. In situ samples of KE3 ((Schoenoplectus tabernaemontani, left) and LV4 (Stuckenia pectinata, right).

Also, visual comparison between averaged SpecimIQ and ASD spectra of the same sample showed large deviations, highlighting the challenge of producing representative reference spectra for one species. Still, ignoring differences in absolute reflectance values and considering only the spectral shape, ASD and SpecimIQ spectra of the same sample often showed similarities. Example spectra two samples are given in Figure 18 and photos of same samples in Figure 18. In Figure 18, spectral range of 350 – 1300 nm is shown to highlight spectral properties in the NIR range. Still, in water applications, due to strong absorption in longer wavelengths, the most important spectral features are in the visible spectral range, 400 – 750 nm. In Appendix 4, both ASD and SpecimIQ spectra of each sample are given.

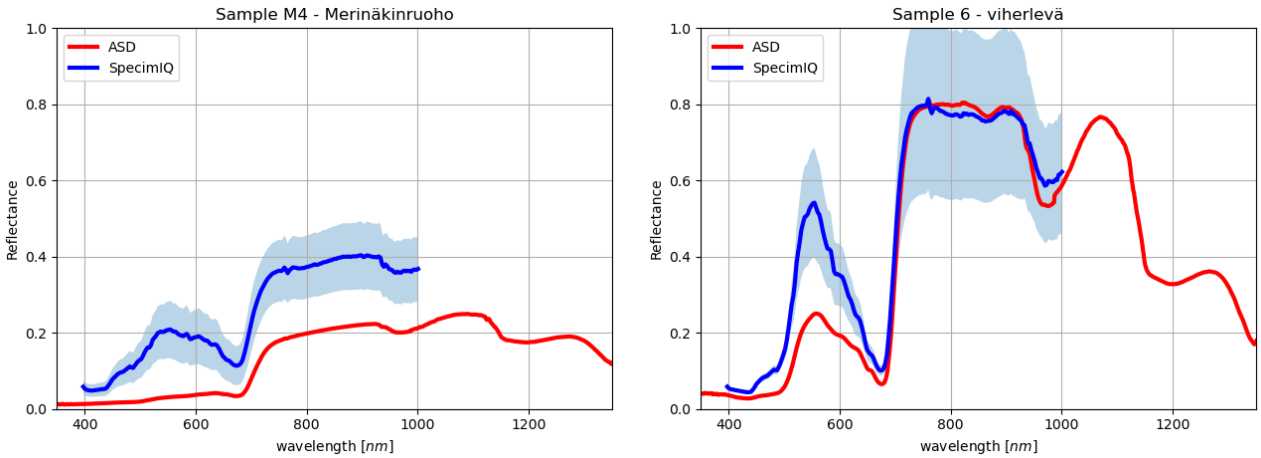

Figure 17. averaged ASD and SpecimIQ spectra of M4 (Najas marina, left) and 6 (Chlorophyta (Ulva sp.), right). Light blue shading on SpecimIQ spectra is +-standard deviation from five different spectra of the same sample.

Figure 18. In situ samples of M4 ((Najas marina, left) and 6 (Chlorophyta (Ulva sp.), right).

To get quantitative values for comparing spectral differences between each sample, spectral angle and Chi-square metrics were calculated between each SpecimIQ sample spectra (Table 3). SAM values varied between 2.4 (M10 (*Zannichellia sp.*) vs. LV2 (*Phragmites australis*)) and 20.5 (PE13 (*Fontinalis sp.*) vs. 6 (*Chlorophyta*)) and were on average 9.8. Chi-square values varied between 0.8 (A1 (*Chara aspera*) vs. AK1 (*Lemna trisulca*)) and 147.4 (JP10 (*Fucus sp.*) vs. PE13 (*Fontinalis sp.*)) and were on average 24.2. In Kaskinen, two different samples of *Fucus sp.* (Hauru) were collected (sample names JP10 & P4). SpecimIQ and ASD spectra of these *Fucus sp*. samples are shown in Figure 19. SAM value of this pair is 4.4 and Chi-square value is 15.0. These values make sense as the spectral shape of both P4 and JP10 are similar resulting low SAM value. Still, SpecimIQ spectra have absolute differences both in VIS and NIR range resulting higher Chi-square value.

Table 3. Spectral angle mapper values (SAM, lower left area) and Chi-square values (Chi2, upper right area) between all averages in situ SpecimIQ sample spectra. Range of SAM is [0,180] and values closer to 0 indicate spectral similarity. SAM values smaller than 5 have green background, values between 5 and 10 have yellow background and values larger than 10 have red background. Chi-square values close to 0 indicate high spectral similarity. Chi-square values smaller than 10 have green background, values between 10 and 30 have yellow background and values larger than 30 have red background.

	Chi2	Haggisgrund						Huljan					Kaskinen						
SAM		A1	AK1	KE3	LV2	M10	MA2	A9	JP28	M4	S5	T4	6	JP07	JP10	P4	K2	LV4	PE13
Haggisgrund	A1		0,8	21,3	14,9	2,1	2,8	21,3	13,5	8,6	47,5	14,7	44,5	10,7	66,4	40,5	50,1	28,2	5,6
	AK1	5,3		19,7	14,1	3,7	4,5	19,2	10,9	8,3	45,4	12,6	42,4	8,7	62,9	36,1	47,0	25,0	4,8
	KE3	4,0	7,5		2,5	32,6	91,0	2,8	12,2	9,8	10,3	6,7	11,6	9,2	29,6	29,6	15,6	11,6	14,9
	LV2	8,3	12,8	5,6		16,0	67,0	7,0	15,6	3,7	16,3	9,5	17,1	9,9	40,3	39,9	24,6	19,0	10,7
	M10	9,4	14,0	6,9	2,4		11,1	18,2	14,2	4,8	40,5	13,6	38,7	9,3	62,3	43,0	45,4	27,7	4,3
	MA2	4,1	4,9	4,4	9,4	10,2		30,3	20,7	15,2	58,2	22,8	55,1	17,3	77,2	48,6	60,6	37,2	11,0
Huljan	A9	3,9	3,0	6,0	11,0	12,1	4,3		4,7	13,2	11,5	1,7	10,7	7,2	24,2	14,9	12,2	3,5	15,8
	JP28	9,7	5,8	11,3	16,2	17,4	9,3	6,4		8,3	20,6	0,9	18,4	2,1	32,3	12,8	19,5	5,0	9,0
	M4	10,5	13,2	9,4	9,0	9,8	11,9	11,0	13,2		24,2	7,8	22,9	5,3	46,0	34,5	30,0	18,5	5,4
	S5	8,9	11,6	7,8	7,9	9,0	10,2	9,3	12,0	3,1		41,1	3,7	55,3	20,8	56,1	11,4	34,2	78,8
	T4	5,2	3,2	7,6	12,4	13,7	6,1	2,5	4,9	11,3	9,7		15,5	3,5	30,8	15,4	18,0	4,6	9,3
Kaskinen	6	12,9	14,9	13,9	14,2	15,3	15,4	12,9	13,9	8,0	8,0	12,1		60,2	20,5	50,0	12,8	26,2	84,7
	JP07	8,2	6,0	7,9	12,9	13,5	5,2	5,9	7,4	12,9	11,5	6,9	16,7		37,6	18,8	23,5	9,0	2,7
	JP10	10,9	7,8	12,1	16,5	17,6	9,8	7,7	4,1	13,3	11,9	6,7	13,8	7,7		15,0	4,5	27,6	147,4
	P4	12,1	7,8	13,6	18,6	19,6	10,5	8,7	5,1	16,5	15,2	8,1	17,3	7,9	4,0		4,6	3,8	59,2
	K2	9,3	6,5	10,3	14,9	15,9	8,4	6,3	3,5	12,0	10,7	5,4	13,5	6,0	3,0	5,1		11,5	84,1
	LV4	8,8	4,2	10,5	15,7	16,9	7,7	5,4	3,5	14,6	13,0	4,6	15,7	5,9	5,1	4,4	4,4		30,2
	PE13	9,3	9,8	8,2	11,6	11,7	6,3	9,5	14,0	16,0	14,4	11,6	20,5	7,6	14,2	13,9	12,9	11,8	

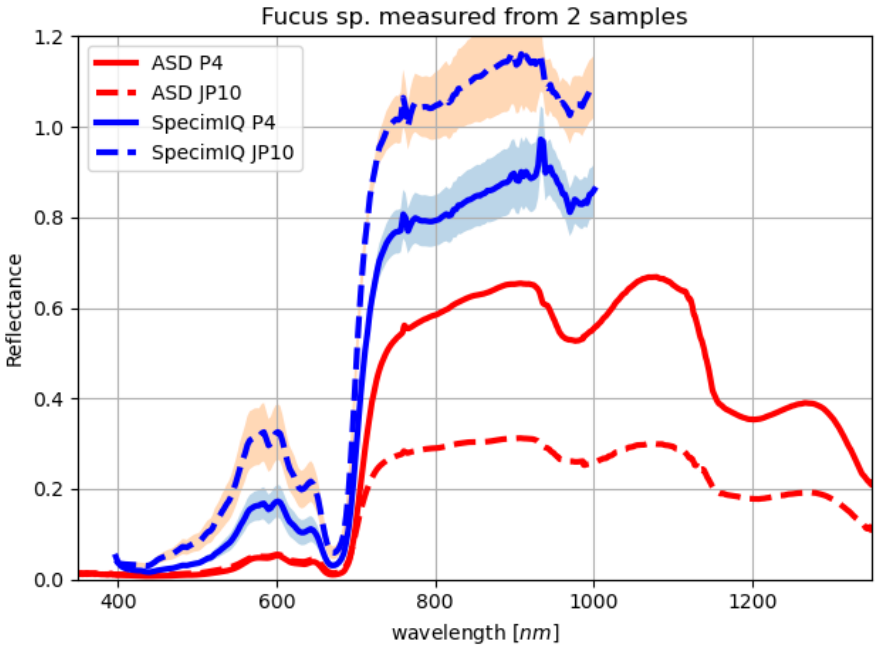

Figure 19. Averaged SpecimIQ and ASD spectra of two Fucus sp. samples P4 and JP10.

4.1.2. Research questions related to *in situ* spectral measurements

Specific research questions related to spectra were related to separability of different species from others. They are discussed in the following paragraphs. Unfortunately, there were no in situ samples of *Ranunculus* species or any *Hippuris* species, so it was not possible to analyze spectra of these species.

Can we define spectral differences between stonewort's (*Characea*, näkinpartaislevät) and vascular plants (mostly *Potamogeton/Stuckenia, Myriophyllum, Ranunculus*)?

Averaged SpecimIQ spectra with standard deviation confidence intervals of two stonewort (samples A1 & MA2) and vascular plants (samples LV4, T4, JP28) are shown in Figure 20 (left). Both stonewort have similar and overlapping spectra, and they differ from vascular plants especially on NIR range in wavelengths above 750 nm. Still stonewort have some differences with vascular plants also in visible spectral range. Spectral angle metrics between the two stonewort, A1 vs. MA2 gave 4.1; A1 vs. vascular plats LV4, T4 and JP28 gave 8.8, 5.2 and 9.7; and MA2 vs. vascular plants 7.7, 6.1 and 9.3 respectively. Chi-square metrics two stonewort, A1 vs. MA2 gave 0.8; A1 vs. vascular plats LV4, T4 and JP28 gave 28.2, 14.7 and 13.5; and MA2 vs. vascular plants 37.2, 22.8 and 20.7 respectively. Based on these metrics, stonewort could be separated from vascular plants based on their spectra.

Do *Potamogeton/Stuckenia* species differ from *Myriophyllum* species?

Averaged SpecimIQ spectra with standard deviation confidence intervals of three *Potagemon/Stucenia* species (samples T4, LV4, S5) and one *Myriophyllum* specie (sample JP28) are shown in Figure 20 (right). Spectra of JP28 overlaps with T4 and partly with LV4, but S5 has different spectral shape especially in VIS spectral range. Spectral angle metrics between *Myriophyllum* (JP28) vs. T4, LV4 and S5 are 4.9, 3.5 and 12.0 respectively. Chi-square metrics between *Myriophyllum* (JP28) vs. T4, LV4 and S5 are 0.9, 5.0 and 20.6 respectively. These values indicate that JP28 could be separated from S5, but not from T4 or LV4.

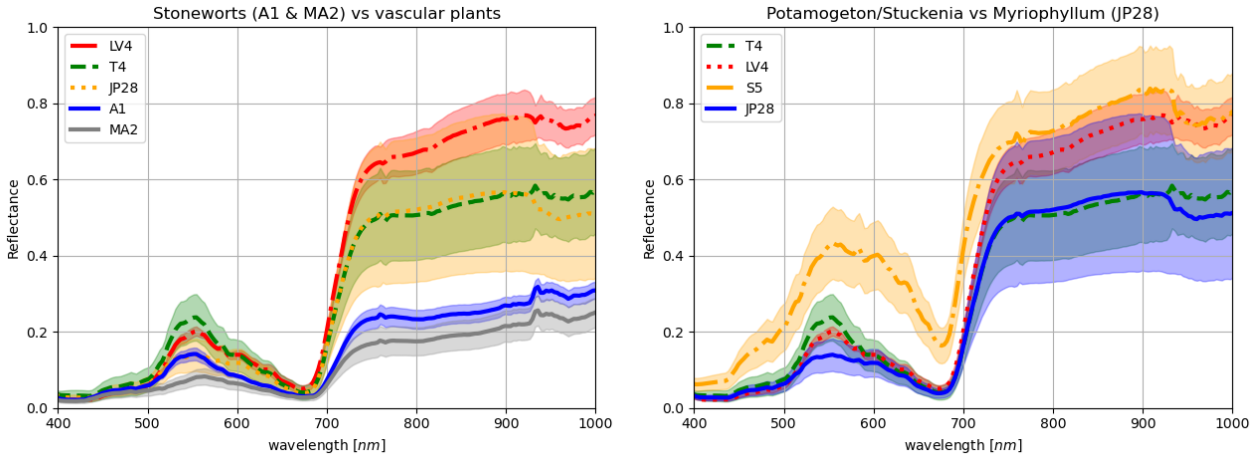

Figure 20. Spectral comparison of different species. Left: stonewort versus vascular plants. Right: Potagemon/Stuckenia versus Myriophyllum. Averaged SpecimIQ sample spectra with standard deviation confidence intervals.

Do sedges (sinikaisla, *Schoenoplectus tabernaemontani*) have different spectral features than reed (ruoko, *Phragmites australis*)?

Averaged SpecimIQ spectra with standard deviation confidence intervals of sedge (KE3) and reed (LV2) samples are given in Figure 21. Both samples have similar spectral shape and reflectance values. Spectral angle metric between sedge (KE3) and reed (LV2) is 5.6, and Chi-square metric 2.5. Separating these two species just based on their spectra seems highly challenging.

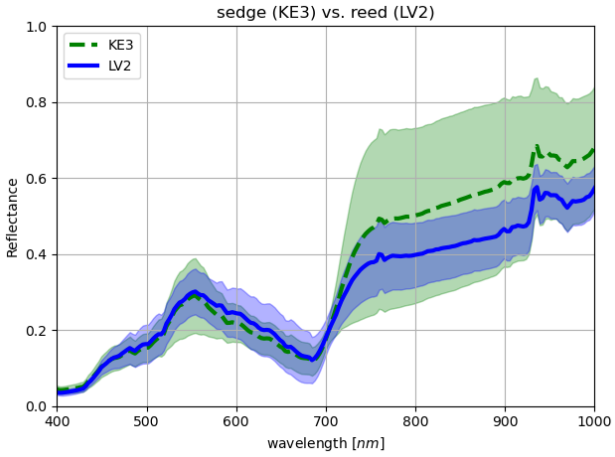

Figure 21. Spectral comparison of Schoenoplectus tabernaemontani (KE3, sedge) and Phragmites australis (LV2, reed). Averaged SpecimIQ sample spectra with standard deviation confidence intervals.

Spectral differences between algae (green algae, brown algae, red algae), stonewort's and vascular plants, mosses?

Averaged SpecimIQ spectra with standard deviation confidence intervals of green algae (6, *Chlorophyta* (*Ulva sp.*)), red algae (JP07, *Rhodophyta*) and moss (PE13, *Fontinalis sp.*) are given in Figure 22, left. Green algae has clearly separable spectra from red algae and moss on both VIS and NIR spectral ranges. Spectral angle metrics between moss (PE13) and green algae (6) is 20.5 and between moss (PE13) and red algae (JP07) is 7.6. Chi-square metrics for same comparisons are 84.4 and 2.7 respectively. Based on these results, mosses should be separable from green algae, but is highly similar to red algae based on their spectra.

Averaged SpecimIQ spectra with standard deviation confidence intervals of green algae (6, *Chlorophyta* (*Ulva sp.*)), red algae (JP07, *Rhodophyta*) and two stonewort (A1, *Chara aspera* and MA2, *Chara tomentosa*) are given in Figure 22, right. Spectral angle metrics between *Chara aspera* (A1) vs. green algae (6) is 12.9, *Chara aspera* (A1) vs. red algae (JP07) is 8.2. Chi-square metrics for same comparisons are 44.5 and 10.7 respectively. Spectral angle metrics between *Chara tomentosa* (MA2) vs. green algae (6) is 15.4, *Chara Tomentosa* (MA2) vs. red algae (JP07) is 5.2. Chi-square metrics for same comparisons are 55.1 and 17.3 respectively. These results show, that it is possible to separate green and red algae from stoneworts.

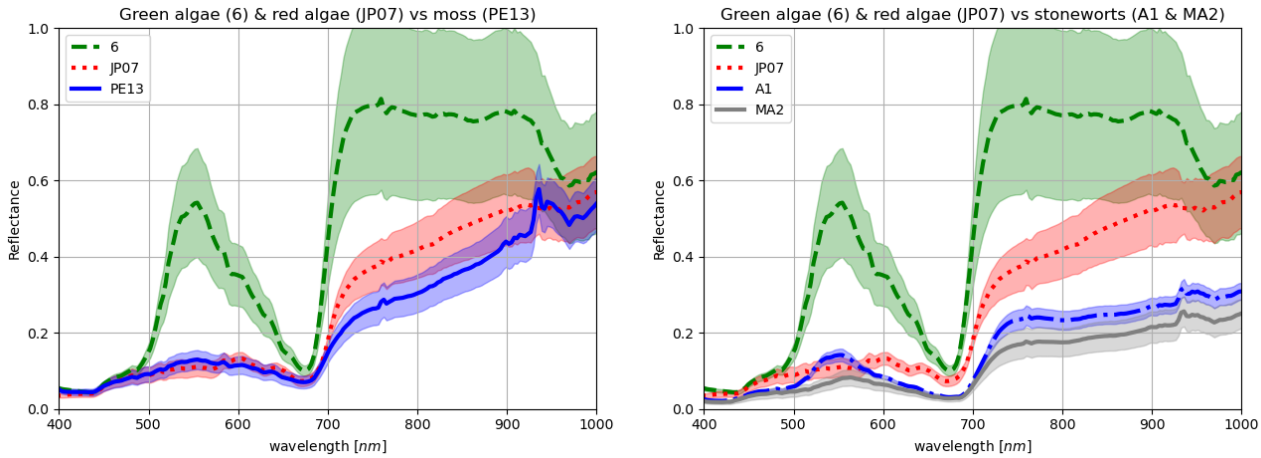

Figure 22. Left: Sample spectra of green algae (6, Chlorophyta (Ulva sp.)), red algae (JP07, Rhodophyta) and moss (PE13, Fontinalis sp.). Right: Spectral comparison of Green (6, Chlorophyta (Ulva sp.)) & red algae (JP07, Rhodophyta) versus two stoneworts (A1 Chara aspera, MA2 Chara tomentosa). Averaged SpecimIQ sample spectra with standard deviation confidence intervals.

4.2. Results from drone data

4.2.1. DTM and DSM results

The Metashape photogrammetric processing produced, along the RGB orthomosaic, also a 3D model of the underwater in shallow water areas. Figure 23 shows the data for the central bay of the Kaskinen area. The Kaskinen 3D data shows reliable, relatively noise free, depth information up to 60-90 cm water depth and usable information up to 1.2 m water depth. These threshold depths may vary in other locations and mapping flights depending at least on the turbidity of water and the amount of waves. Figure 24Figure 25 show similar datasets for Huljan and Haggisgrund. In both areas, the underwater 3D data is reliable, and the underwater vegetation can be clearly detected in water depths up to 60-80 cm. In these areas, the width, depth, height, and shapes of different algae zones can be measured reliably. In the deeper areas (>1 m) or areas affected by waves, e.g. in Huljan in the center of the bay and in Haggisgrund in the south corner of the area, the photogrammetric point clouds get noisy and extracting reliable 3D information gets difficult.

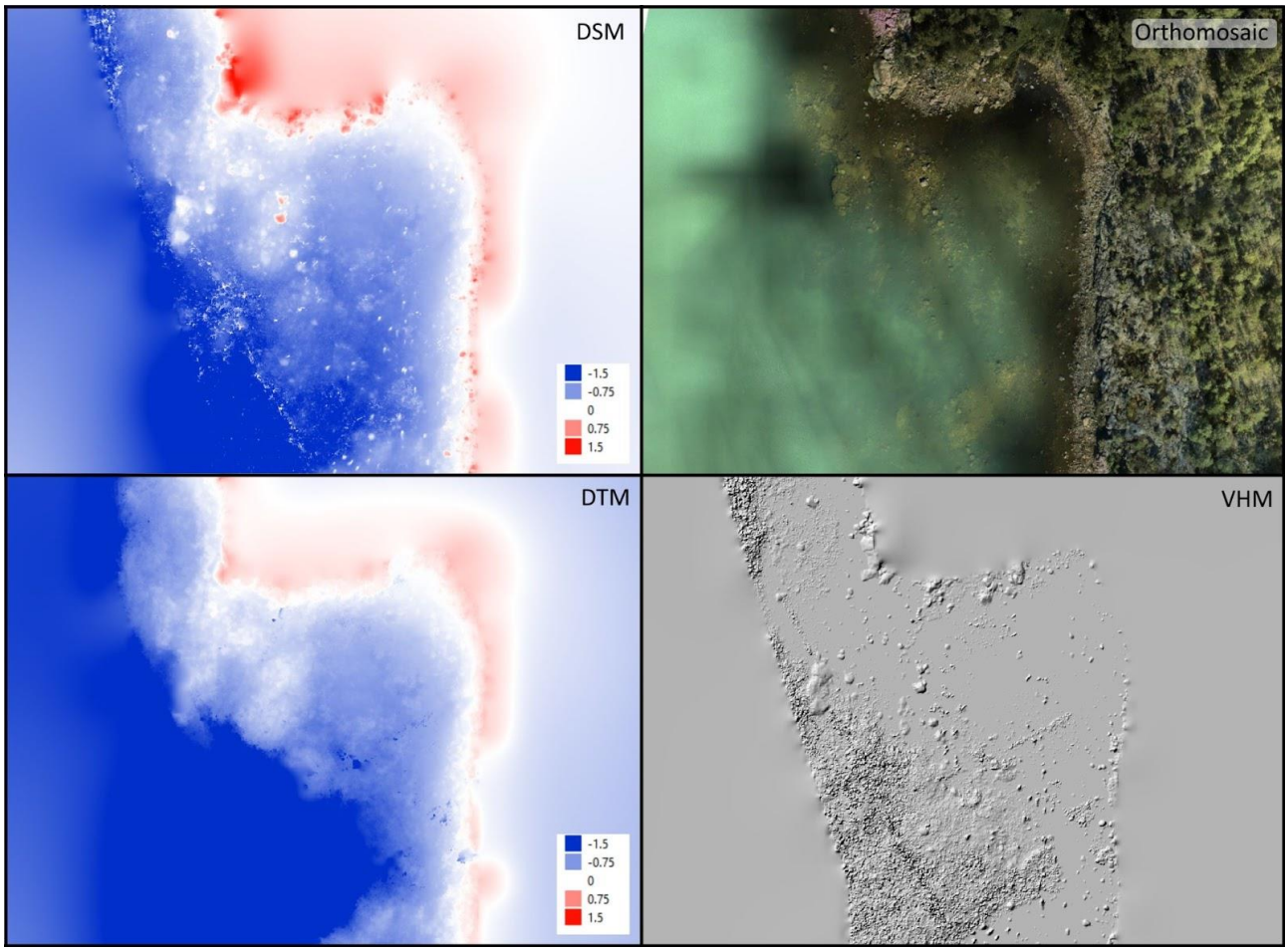

Figure 23. Kaskinen photogrammetric data products produced from the RGB images. Top left: Digital Surface Model showing top of underwater vegetation; Top right: RGB orthomosaic; Bottom left: Digital Terrain Model extracted from the photogrammetric point cloud depicting bottom soil under the vegetation and protruding stones; Bottom right: Vegetation Height Model as difference between DSM and DTM.

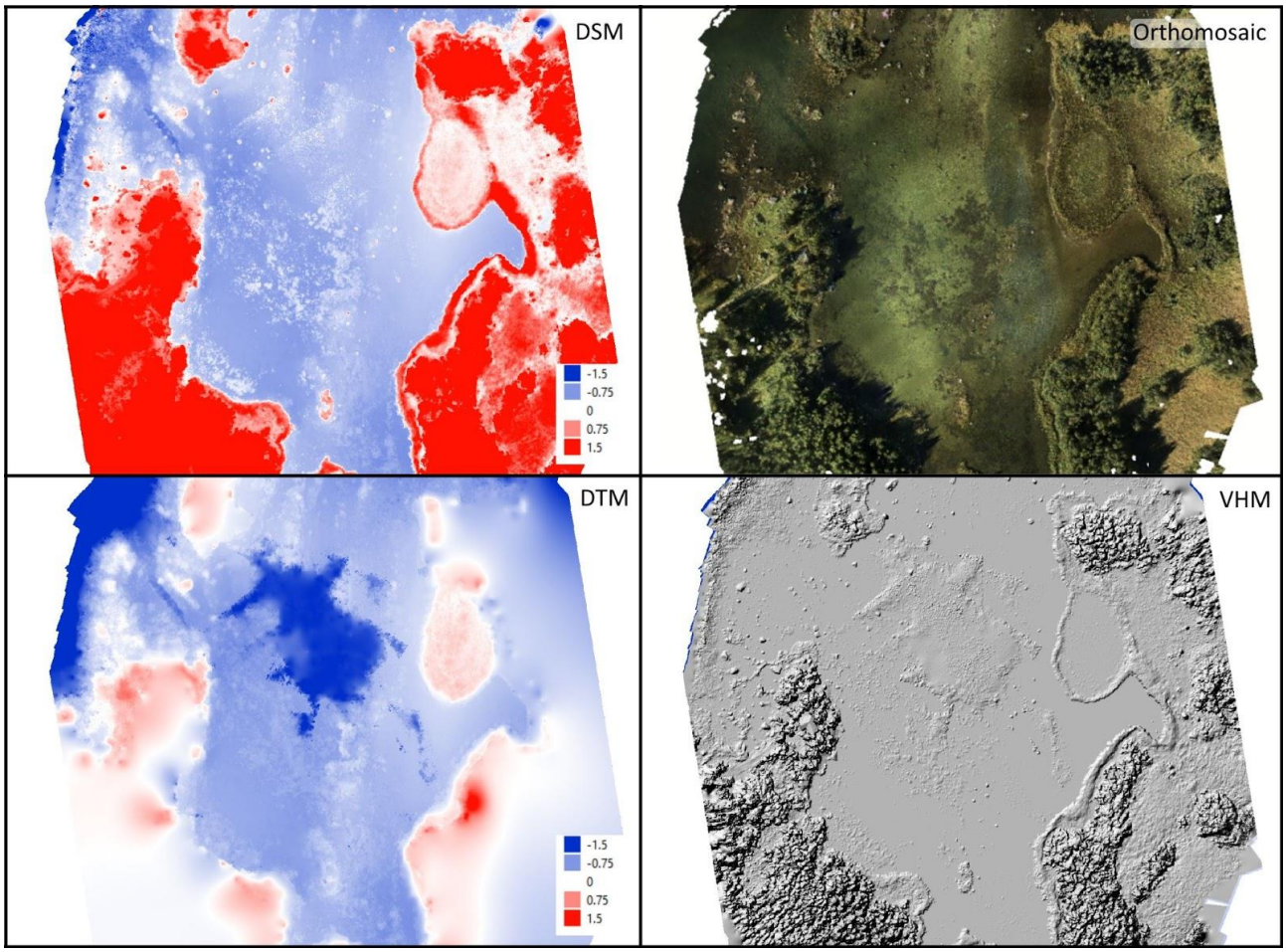

Figure 24. Huljan photogrammetric data products produced from the RGB images. Top left: Digital Surface Model showing top of underwater vegetation; Top right: RGB orthomosaic; Bottom left: Digital Terrain Model extracted from the photogrammetric point cloud depicting bottom soil under the vegetation and protruding stones; Bottom right: Vegetation Height Model as difference between DSM and DTM.

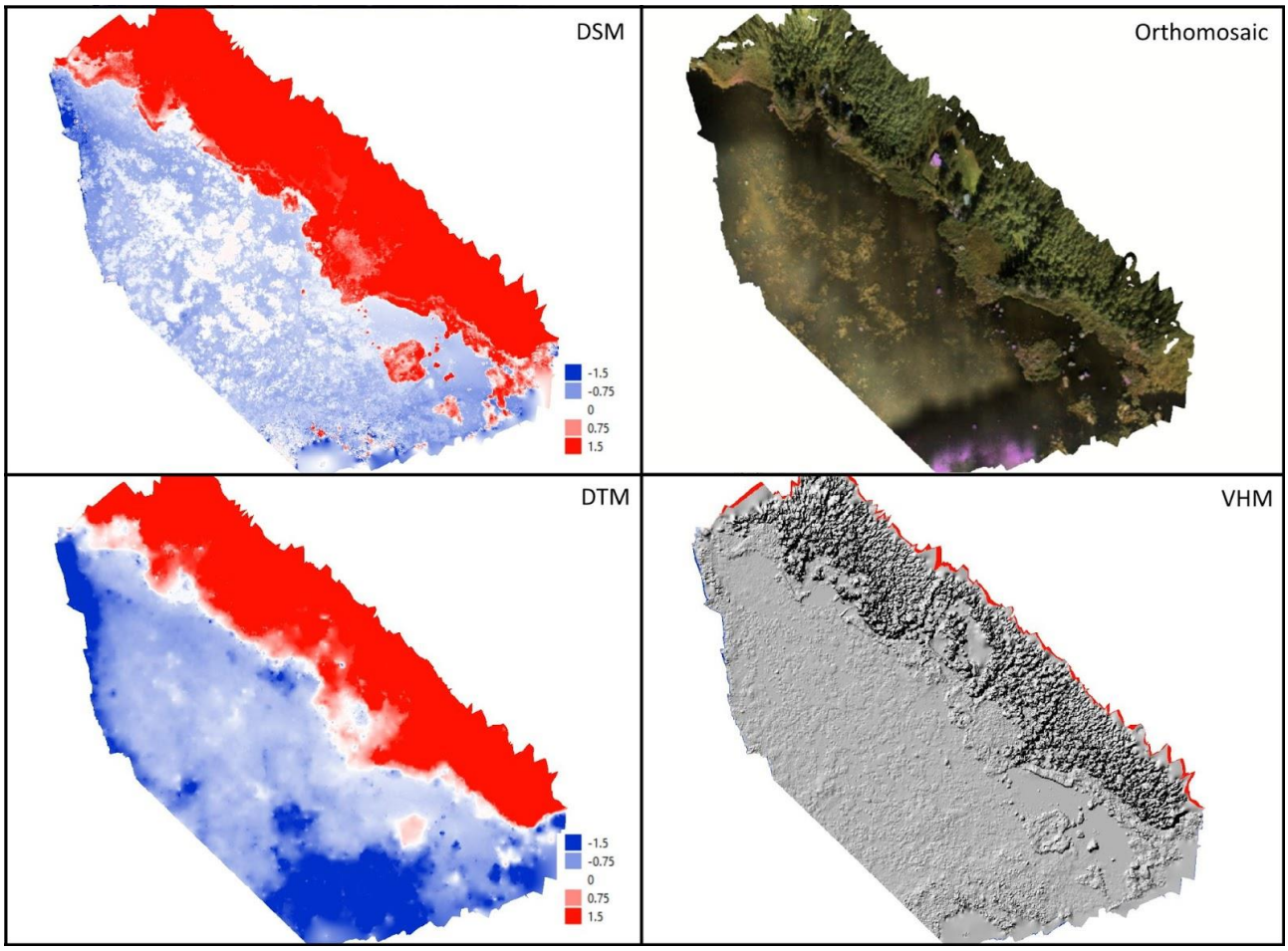

Figure 25. Haggisgrund photogrammetric data products produced from the RGB images. Top left: Digital Surface Model showing top of underwater vegetation; Top right: RGB orthomosaic; Bottom left: Digital Terrain Model extracted from the photogrammetric point cloud depicting bottom soil under the vegetation and protruding stones; Bottom right: Vegetation Height Model as difference between DSM and DTM.

4.2.2. Comparison of image derived spectra to *in situ* reference

Average spectra from each *in situ* locations was measured from REHU VIS image mosaics from the area 0.8 m diameter circle. Measured in situ image spectra form each three areas are shown in Figure 26. Spectral values were close to 0 or even slightly negative for some locations where vegetation was under water. Spectral range of Kaskinen spectra was between -0.01 and 0.011, between 0.01 and 0.025 for Huljan and between -0.005 and 0.09 for Haggisgrund. These values indicate that the Kaskinen data set was underexposed i.e. the exposure time of the VIS camera was too short during the imaging campaign. The exposure time was adjusted between first and second flights in Kaskinen, but apparently not enough. Exposure time was further adjusted before the last flight in Haggisgrund. Also, the Kaskinen area, the water was much deeper than in other two areas, which also dampens the spectra of sea bottom vegetation. In Haggisgrund data, one sample spectra, the reed (Phragmites australis, LV2), stands out from other spectra. This is due to fact that the reed is clearly above water, whereas other targets are more or less under the water.

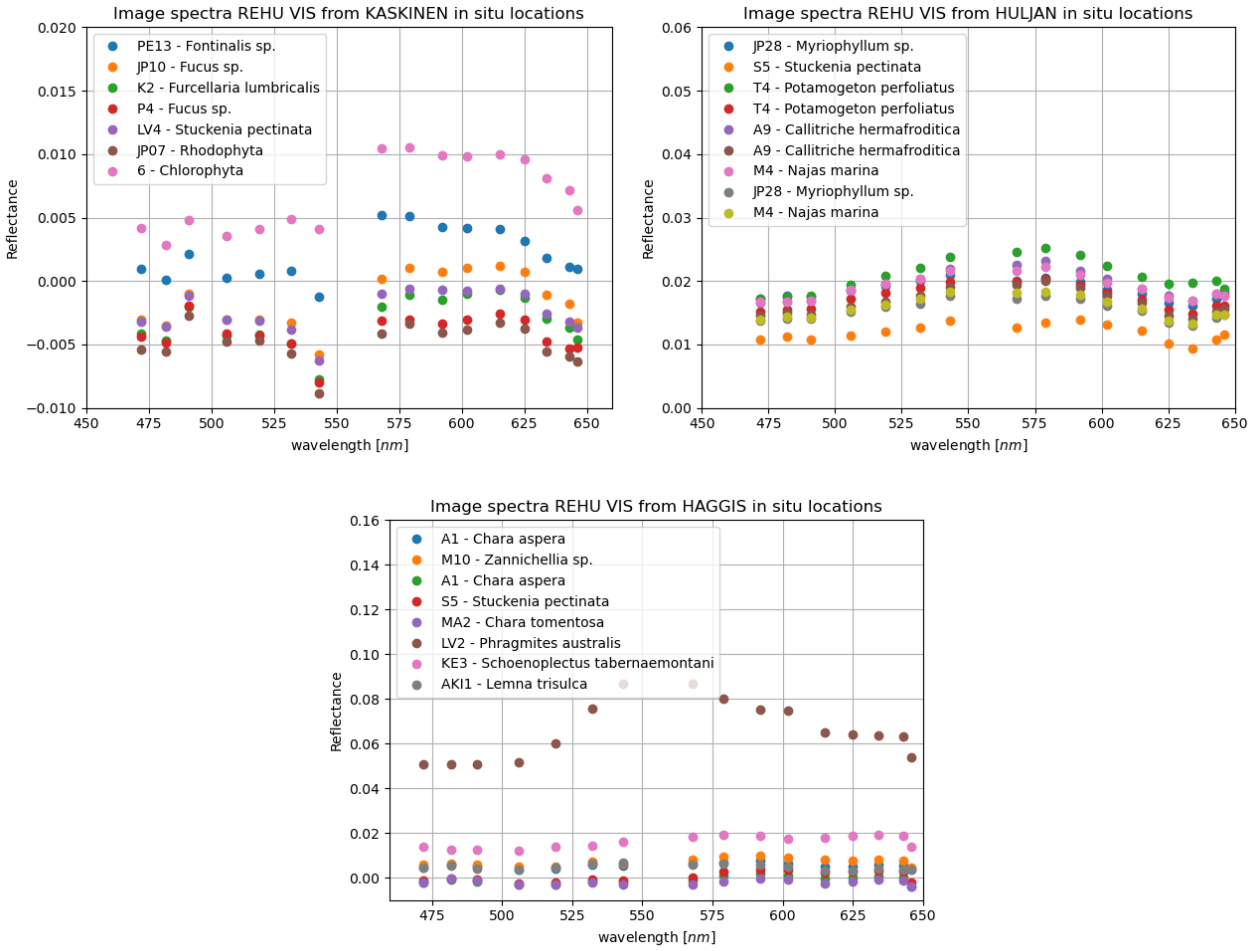

Figure 26. Image derived spectra from in situ locations of Kaskinen (top left), Huljan (top right) and Haggisgrund (bottom).

Visualization of image derived REHU VIS sample spectra in comparison to in situ reference spectra measured with SpecimIQ and ASD are shown for samples *Myriophyllum sp.* (JP28) and *Najas Marina* (M4) in Figure 27. Image derived REHU VIS spectral values are clearly lower than SpecimIQ reference spectra, but bit closer to ASD reference spectra. Image derived spectra of all samples are given in Appendix 4.

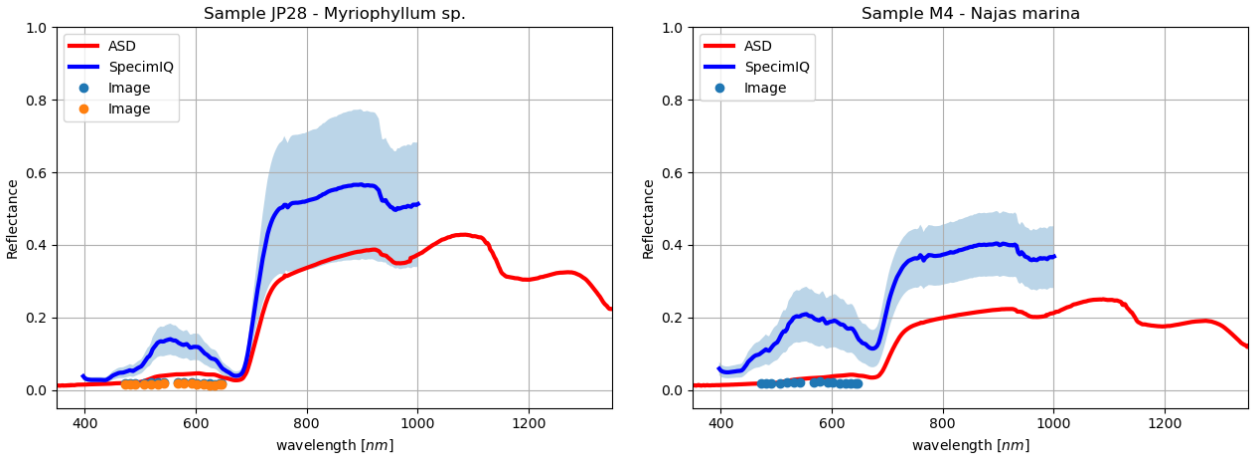

Figure 27. Image derived REHU VIS spectra and in situ reference SpecimIQ and ASD spectra for samples JP28 (Myriophyllum sp., left) and M4 (Najas Marina, right).

Spectral angle mapper (SAM) and modified SAM (msam) metrics were calculated between each *in situ* reference spectra and image derived REHU VIS spectra from *in situ* locations (Table 4 Table 5). These tables show that neither SAM nor msam are able to classify image derived spectra correctly. When comparing only Kaskinen data, all image spectra would be classified to P4 (Fucus sp.), this is correct only for sample P4 itself and JP10, that is also same specie *Fucus sp.*, but different individual. For Huljan data, all image spectra would be classified as M4 (*Najas Marina*) using SAM. With msam, most of the Huljan image derived *in situ* sample spectra would be classified as JP28. For Haggisgrund data, classification results with SAM and msam deviated, but both would classify correctly only sample LV2 (*Phragmites australis*), the reed, that was the only sample clearly above water.

Table 4. Spectral angle mapper SAM values between in situ reference spectra (columns) and image derived spectra (rows). Values closer to 0 indicate spectral similarity. Values between same sample are bordered. Smallest SAM value for each image sample spectra inside same area are on bold. For example, Haggisgrund image derived spectra of sample A1 would be classified as MA2.

				IN SITU REFERENCE SPECTRA																	
				Huljan					Kaskinen							Haggisgrund					
		RefID	Sample	JP28	M4	A9	T4	S5	6	K2	P4	JP10	LV4	JP07	PE13	AK1	A1	M10	MA2	KE3	LV2
IMAGE SPECTRA FROM REHU VIS	Kaskinen	1	PE13	39,26	40,30	41,58	41,56	38,40	40,08	38,04	**30,99**	32,06	39,13	40,02	40,92	42,31	42,32	40,33	39,04	40,62	39,85
		2	JP10	122,8	123,9	125,0	124,7	122,0	122,8	121,0	**114,1**	115,4	122,4	123,3	124,6	125,9	125,9	124,1	123,2	124,6	123,7
		3	K2	147,2	148,2	149,1	148,6	146,5	146,8	145,5	**138,7**	140,0	146,7	147,5	148,9	149,8	149,9	148,4	147,4	148,9	148,1
		4	P4	159,5	160,8	160,2	159,5	159,5	158,3	159,1	**152,8**	154,0	159,0	160,1	161,0	160,4	160,6	160,6	159,5	161,1	160,6
		5	LV4	144,3	145,5	146,0	145,5	143,8	143,9	143,1	**136,3**	137,5	143,9	144,8	146,0	146,5	146,7	145,5	144,4	146,0	145,3
		6	JP07	161,0	162,7	161,5	160,7	161,3	159,4	160,8	**154,6**	155,8	160,4	162,1	162,9	161,7	161,9	162,5	161,3	162,9	162,5
		7	6	19,07	19,32	22,15	22,57	17,27	20,99	16,37	**9,56**	10,73	19,19	19,17	20,38	23,28	23,12	19,77	19,19	20,14	19,18
	Huljan	8	JP28	6,74	**4,19**	8,57	10,35	6,26	11,39	7,50	14,12	12,72	9,59	4,40	2,72	8,27	8,05	3,46	4,44	4,02	4,31
		9	S5	6,16	**4,75**	8,33	9,92	5,89	10,74	6,82	12,91	11,55	8,88	4,99	3,95	8,16	7,97	4,02	4,24	4,38	4,46
		10	T4	3,70	**2,41**	6,77	8,41	2,61	8,71	4,57	10,60	9,13	6,46	4,44	2,91	7,18	6,93	2,14	2,04	2,26	1,68
		11	T4	4,88	**3,32**	7,00	8,75	4,76	9,57	6,45	12,74	11,29	7,74	4,70	2,54	6,90	6,69	2,47	2,75	2,71	2,97
		12	A9	4,27	**2,96**	6,80	8,48	3,81	9,08	5,71	11,62	10,16	7,04	4,63	2,71	6,92	6,70	2,27	1,97	2,31	2,25
		13	A9	4,71	**3,71**	7,01	8,64	4,54	9,36	6,25	11,98	10,54	7,41	4,97	3,19	6,98	6,78	2,90	2,35	2,88	2,95
		14	M4	4,84	**2,71**	7,23	8,99	4,26	9,71	5,91	12,32	10,88	7,72	4,12	2,01	7,26	7,02	1,98	2,66	2,43	2,49
		15	JP28	5,61	**3,85**	7,62	9,34	5,37	10,24	6,84	13,08	11,66	8,41	4,69	2,85	7,43	7,23	3,03	3,36	3,34	3,58
		16	M4	4,94	**3,64**	7,00	8,70	4,90	9,55	6,54	12,71	11,27	7,70	4,91	2,91	6,87	6,66	2,79	2,83	2,86	3,13
	Haggisgrund	17	A1	9,61	9,07	12,42	13,41	8,26	13,33	8,01	9,57	8,71	11,12	8,59	9,26	12,81	12,64	8,96	**8,45**	9,19	8,56
		18	M10	10,57	10,17	13,96	14,86	8,65	14,11	7,65	6,44	6,03	11,81	9,70	10,89	14,74	14,54	10,40	10,06	10,86	**9,96**
		19	A1	118,3	119,5	120,1	119,6	117,5	117,9	116,2	110,2	111,4	117,5	119,0	120,3	121,0	121,0	119,7	119,0	119,9	**119,2**
		20	S5	72,44	72,78	75,03	75,01	70,94	73,22	69,20	63,59	64,87	72,09	72,11	73,82	76,22	76,07	73,30	**73,13**	73,73	72,82
		21	MA2	152,4	153,0	153,5	153,0	151,9	152,1	150,5	145,9	147,0	152,0	151,9	153,3	153,8	153,9	153,0	152,5	153,3	152,8
		22	LV2	3,10	5,35	5,09	5,97	3,65	5,76	5,87	10,06	8,62	3,11	8,07	6,52	6,15	5,89	5,48	4,60	4,31	**4,15**
		23	KE3	9,32	7,15	12,76	14,05	6,30	13,54	5,20	7,91	7,08	10,95	6,63	8,08	13,65	13,35	7,90	8,61	8,54	**7,57**
		24	AKI1	9,80	11,16	9,04	9,36	11,26	10,72	12,88	16,69	15,42	10,14	12,59	10,81	**8,34**	8,39	10,48	9,26	9,46	9,99

Table 5. Modified spectral angle mapper msam values between in situ reference spectra (columns) and image derived spectra (rows). Values closer to 1 indicate spectral similarity. Values between same sample are bordered. Largest msam value for each image sample spectra inside same area are on bold. For example, Haggisgrund image derived spectra of sample A1 would be classified as MA2.

				IN SITU REFERENCE SPECTRA																	
				Huljan					Kaskinen							Haggisgrund					
		RefID	Sample	JP28	M4	A9	T4	S5	6	K2	P4	JP10	LV4	JP07	PE13	AK1	A1	M10	MA2	KE3	LV2
IMAGE SPECTRA FROM REHU VIS	Kaskinen	1	PE13	0,27	0,28	0,12	0,13	0,38	0,19	0,41	**0,63**	0,62	0,25	0,49	0,25	0,08	0,08	0,28	0,35	0,21	0,29
		2	JP10	0,16	0,19	-0,01	-0,01	0,29	0,07	0,37	**0,55**	0,52	0,12	0,46	0,14	-0,06	-0,06	0,17	0,20	0,08	0,17
		3	K2	0,07	0,09	-0,09	-0,09	0,18	-0,02	0,26	**0,44**	0,42	0,03	0,36	0,05	-0,13	-0,13	0,08	0,12	-0,01	0,08
		4	P4	-0,04	-0,05	-0,15	-0,15	0,01	-0,11	0,04	**0,21**	0,19	-0,09	0,15	-0,04	-0,15	-0,16	-0,02	0,04	-0,10	-0,05
		5	LV4	0,09	0,09	-0,06	-0,06	0,18	0,00	0,24	**0,42**	0,40	0,04	0,34	0,07	-0,09	-0,10	0,10	0,15	0,01	0,09
		6	JP07	-0,02	-0,03	-0,12	-0,13	0,03	-0,09	0,06	**0,21**	0,19	-0,07	0,17	-0,01	-0,13	-0,14	0,00	0,06	-0,08	-0,03
		7	6	0,33	0,39	0,16	0,17	0,50	0,26	0,58	**0,78**	0,76	0,33	0,63	0,30	0,10	0,10	0,34	0,35	0,28	0,37
	Huljan	8	JP28	0,59	0,49	**0,68**	0,67	0,43	0,63	0,28	0,19	0,22	0,58	0,26	0,60	0,72	0,71	0,58	0,63	0,62	0,56
		9	S5	**0,58**	0,48	0,56	0,56	0,48	0,56	0,40	0,32	0,35	0,55	0,40	0,56	0,57	0,56	0,56	0,61	0,57	0,55
		10	T4	**0,82**	0,78	0,70	0,70	0,80	0,77	0,62	0,54	0,58	0,81	0,61	0,80	0,64	0,65	0,82	0,82	0,79	0,84
		11	T4	0,73	0,64	**0,74**	0,74	0,60	0,74	0,43	0,34	0,38	0,71	0,42	0,75	0,74	0,74	0,73	0,77	0,74	0,71
		12	A9	**0,78**	0,70	0,73	0,73	0,69	0,76	0,51	0,45	0,49	0,77	0,50	0,78	0,70	0,70	0,77	0,84	0,78	0,78
		13	A9	**0,72**	0,62	0,69	0,70	0,62	0,71	0,46	0,41	0,45	0,70	0,46	0,71	0,68	0,68	0,71	0,80	0,72	0,71
		14	M4	**0,78**	0,69	0,76	0,76	0,66	0,78	0,49	0,40	0,44	0,76	0,47	0,79	0,73	0,73	0,77	0,80	0,78	0,76
		15	JP28	0,66	0,56	**0,69**	**0,69**	0,53	0,67	0,38	0,31	0,35	0,64	0,38	0,67	0,70	0,69	0,65	0,71	0,68	0,64
		16	M4	0,71	0,61	0,72	**0,72**	0,58	0,72	0,43	0,34	0,38	0,69	0,42	0,71	0,73	0,72	0,70	0,75	0,72	0,69
	Haggisgrund	17	A1	0,38	0,37	0,27	0,28	0,45	0,32	0,47	0,55	0,55	0,38	0,52	0,36	0,24	0,24	0,38	**0,43**	0,36	0,42
		18	M10	0,39	0,42	0,23	0,24	0,53	0,31	0,60	0,71	0,71	0,38	0,67	0,36	0,18	0,18	0,40	0,41	0,34	**0,43**
		19	A1	0,20	0,23	0,04	0,05	0,32	0,12	0,44	0,54	0,52	0,18	0,52	0,17	-0,01	0,00	0,20	0,21	0,14	**0,22**
		20	S5	0,17	0,24	0,01	0,01	0,33	0,09	0,49	0,57	0,54	0,16	0,54	0,15	-0,06	-0,05	0,18	0,16	0,11	**0,20**
		21	MA2	-0,06	-0,05	-0,16	-0,15	0,01	-0,12	0,12	0,19	0,18	-0,08	0,19	-0,07	-0,17	-0,17	-0,05	**-0,03**	-0,10	-0,04
		22	LV2	0,81	0,81	0,72	0,74	0,82	0,80	0,63	0,52	0,56	0,87	0,57	0,78	0,66	0,66	0,80	0,76	0,84	**0,90**
		23	KE3	0,34	0,43	0,20	0,20	0,53	0,29	0,62	0,69	0,68	0,36	0,60	0,32	0,12	0,13	0,35	0,31	0,30	**0,40**
		24	AKI1	0,47	0,37	0,54	0,55	0,36	0,50	0,23	0,19	0,22	0,49	0,21	0,47	0,57	**0,57**	0,46	0,53	0,53	0,48

As a simple example, pixel-wise spectral angle mapping was performed for Huljan and Haggisgrund hyperspectral mosaics. Each water pixel in image was compared to 11 soft bottom reference sample spectra, and closest match based on spectral angle was chosen. Result of these SAM classifications with 11 classes are shown in Figure 28. For Huljan SAM provided mixed results with variety of classes all around the area, but for Haggisgrund, almost whole area was classified to only one class.

As another classification example, pixel-wise SAM results for single class were evaluated. For Kaskinen, potential areas of *Chlorophyta,* green algae*,* was mapped. Map of whole area and zoomed map to most potential areas are shown in Figure 29.

For Haggisgrund, potential areas of *Chara Aspera* were mapped. Map of whole area and zoomed map to most potential areas for Chara Aspera are shown in Figure 30. Potential areas of *Chara Aspera* were mapped also for Huljan area. Map of whole area and zoomed map to most potential areas are shown in Figure 31. *Chara aspera* was chosen for this example as *in situ* samples of *Chara Aspera* were found in Haggisgrund area, but not in Huljan. Historical data tells that Chara aspera has been found from Huljan before, in 2017, but now it seems to be disappeared. SAM mapping of *Chara aspera* in Figure 30 matches well with *in situ* sample locations in Figure 8. Map in Figure 31 shows where existence of *Chara Aspera* should be checked in Huljan area with field trip.

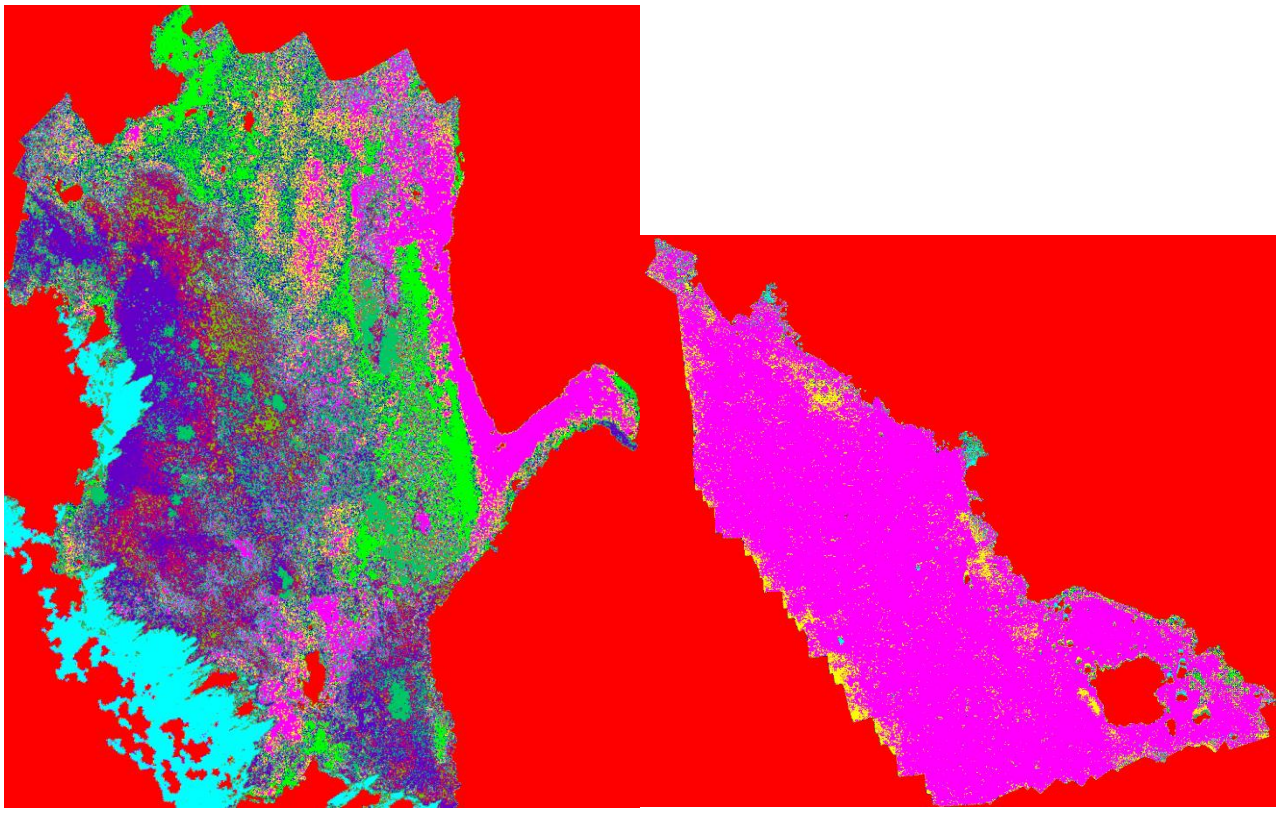

Figure 28. SAM classification results for Huljan (left) and Haggisgrund (right) areas.

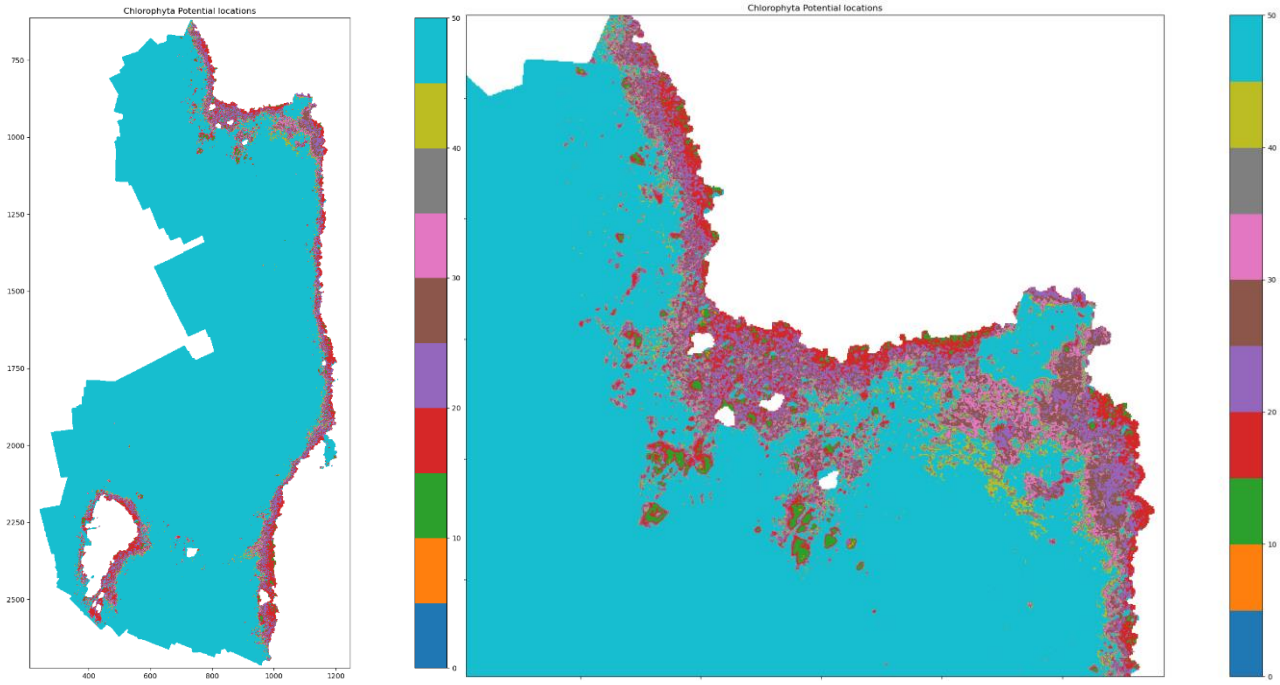

Figure 29. Kaskinen SAM results for most potential areas of green algae (Chlorophyta). Whole area (left), zoomed to top part of the area (left). Scale of the SAM values in these maps is [0,50], and most potential areas for green algae are shown in green (SAM between 10 and 15), red (SAM between 15 and 20) and purple (SAM between 20 and 25) colors.

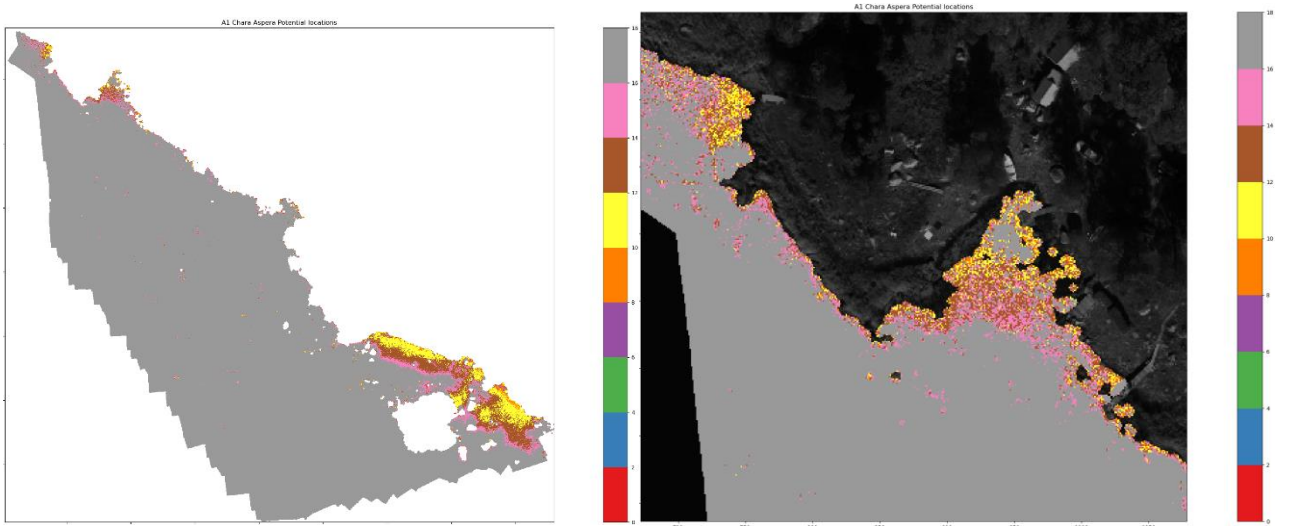

Figure 30. Haggisgrund results for most potential areas of Chara aspera. Whole area (left), zoomed to top part of the area (left). Scale of the SAM values in these maps is [0,18], and most potential areas for Chara aspera are shown in yellow, brown and purple colors (SAM values between 10 and 16).

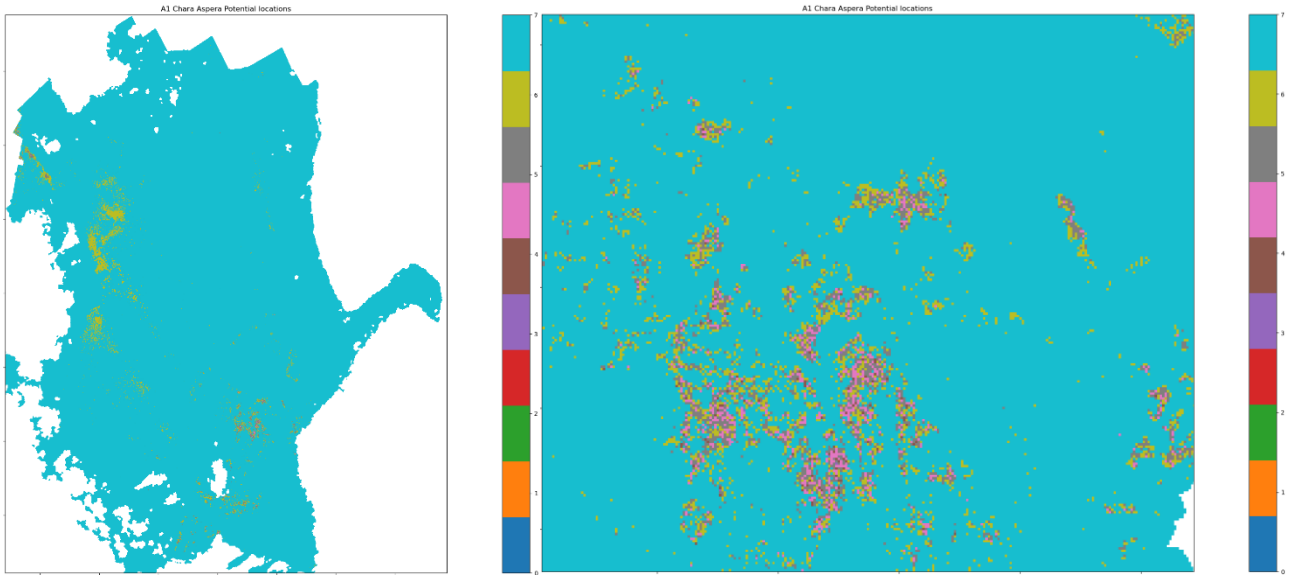

Figure 31. Huljan SAM results for most potential areas of Chara aspera. Whole area (left), zoomed to top part of the area (left). Scale of the SAM values in these maps is [0,7], and most potential areas for Chara aspera are shown in light green, grey and pink colors (SAM values between 4 and 6.5).

4.2.3. Segmentation results

Image mosaic segmentation was tested using three different algorithms from the Scikit-image Python package: felzenszwalb, slic and quickshift. None of the algorithms accepted REHU VIS hyperspectral reflectance data as such, but it had to be converted to 3-band image. This was done by choosing bands 11 (625 nm as red band), 13 (532 nm as green) and 2 (491 as blue) to create RGB image mosaic of each area. Also, as REHU VIS reflectance values over water were close to 0 or sometimes even negative, some image histogram adjustment was done to improve image quality. We used adaptive histogram equalization from Scikit-image package (Adapthist 2021). Finally, land areas were masked out from the image segmentation. Visualizations of each image mosaic after adaptive histogram equalization and masking are shown in Figure 32, Figure 33, Figure 34. Masking of land from Huljan image mosaic was not completely successful, as some forested area remained in the image after masking (Figure 33).

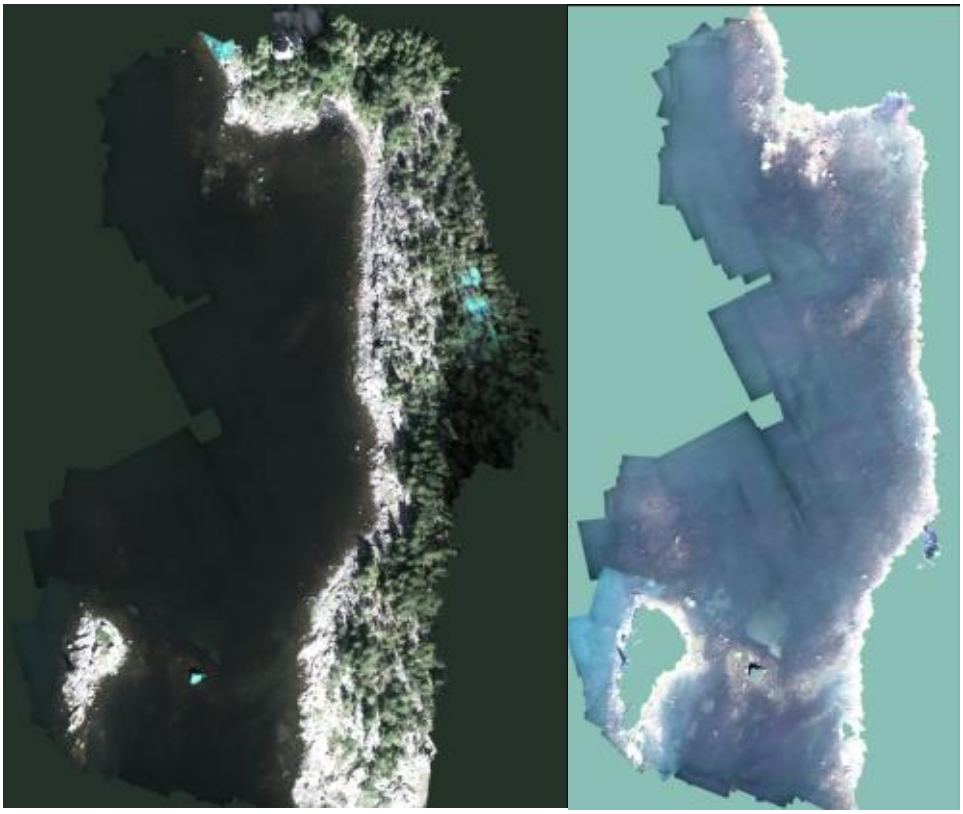

Figure 32. Kaskinen 3-band REHU VIS image used for segmentation, before (left) and after masking (right).

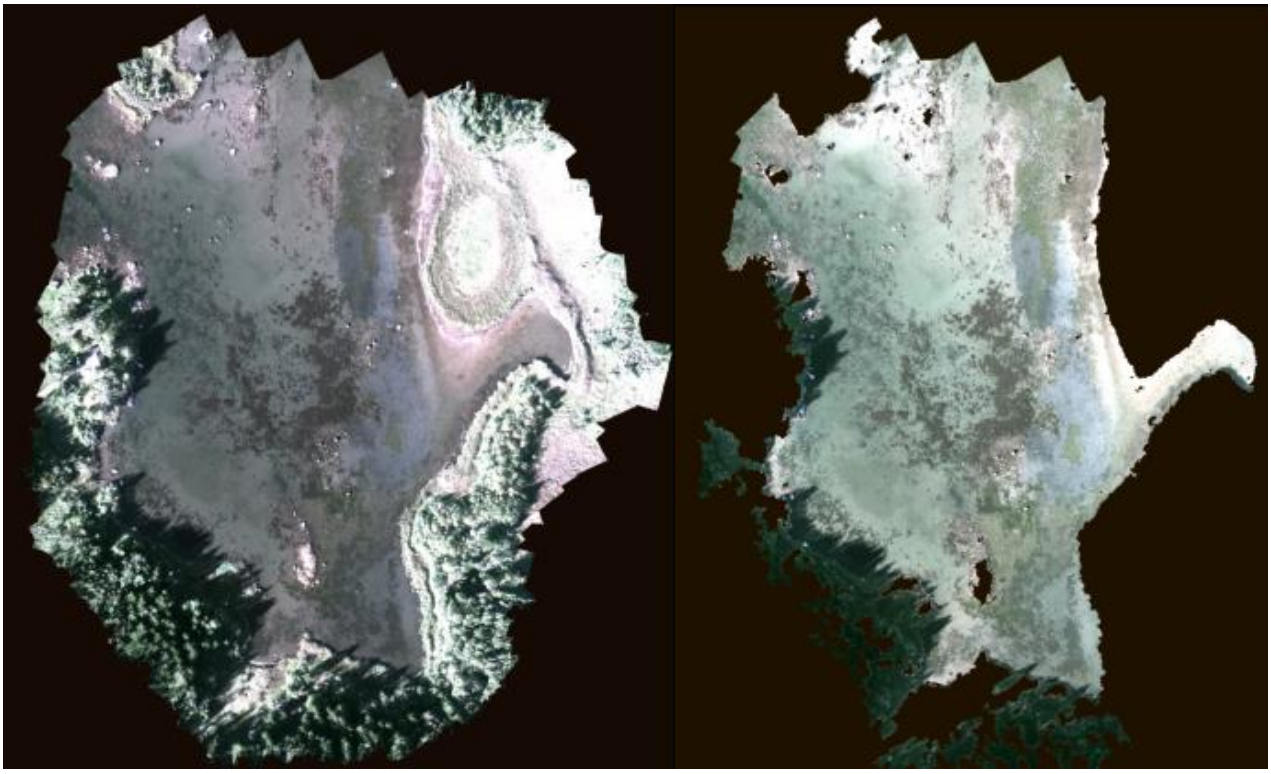

Figure 33. Huljan 3-band REHU VIS image used for segmentation, before (left) and after masking (right).

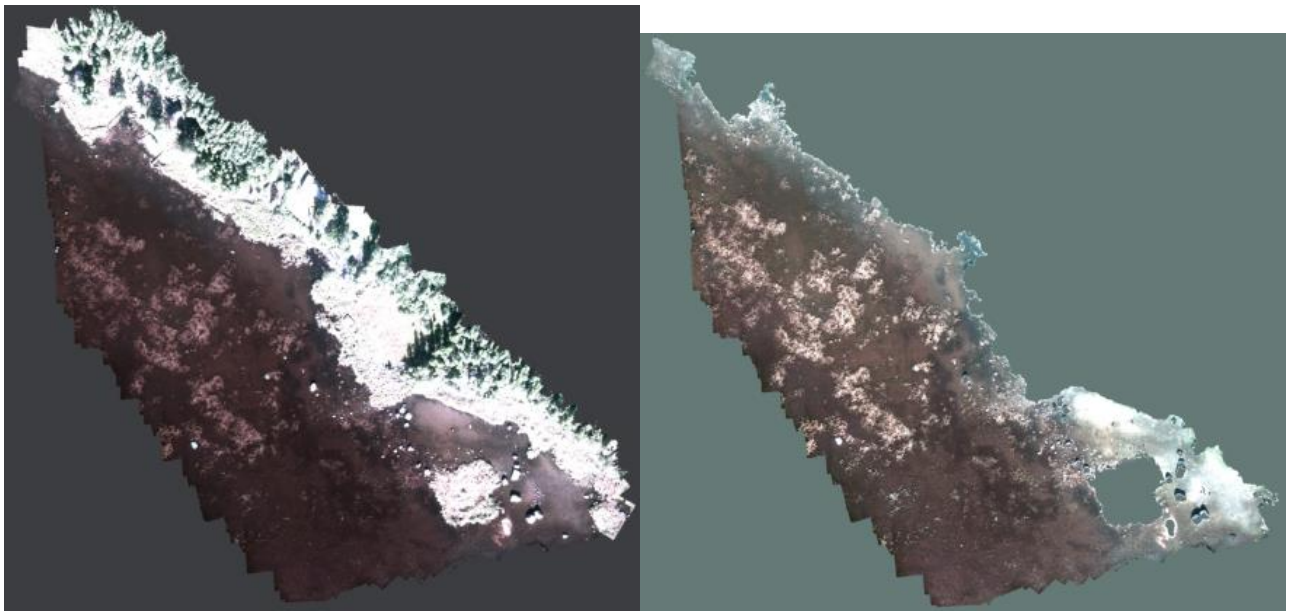

Figure 34. Haggisgrund 3-band REHU VIS image used for segmentation, before (left) and after masking (right).

Typically, felzenszwalb over segments the area to several small segments. But if felzenszwalb algorithm cannot find any suitable segment border, it will not force segments. Slic algorithm tries to create approximately as many segments as given in input parameters. Slic often creates realistic segment borders, but if it cannot find any useful features, slic will create straight segment borders to match the required segment count. This means that slic can create artificial segments without connection to image data. Quickshift algorithm works somehow between felzenszwalb and slic, even though the algorithm itself is unique.

All areas were segmented using felzenszwalb algorithm. Examples of felzenszwalb segmentation of Kaskinen area are shown in Figure 35. This classification seems to be relatively realistic, but there still exists some visible structures around *in situ* location PE13 that are not found. It is difficult to judge if those structures should be segmented as own segments or not. Also, felzenszwalb fails to create any segments on the center part of Kaskinen area. This might be due to underexposure of REHU VIS images, meaning that there is only very little or no information on deeper water areas. Example of the whole Huljan area segmented with felzenszwalb algorithm and zoomed detail is given in Figure 36. Example of the whole Haggisgrund area segmented with felzenszwalb algorithm and zoomed detail is given in Figure 37.

Finally, examples of quickshift segmentation of Haggisgrund area is given in Figure 38 (left), and example of slic segmentation of Kaskinen area is given in Figure 38 (right). The quickshift segmentation of Haggisgrund seems reasonable at first sight, but there are several strange segment borders between some textured areas, or segment borders in completely dark areas. The slic segmentation of Kaskinen area shows that slic can find reasonable segment borders near coastline, but segments in the open water area are clearly artificial.

These segmentation examples show that in principle, it is possible to perform good segmentation of the desired shallow water area in a such way that segments would describe the sample patch sizes automatically. But it is challenging to perform reliable and high-quality segmentation in practice. It requires iterating several parameters over a large value range, trial and error, and, most importantly, expert operator with understanding of biology and species under evaluation.

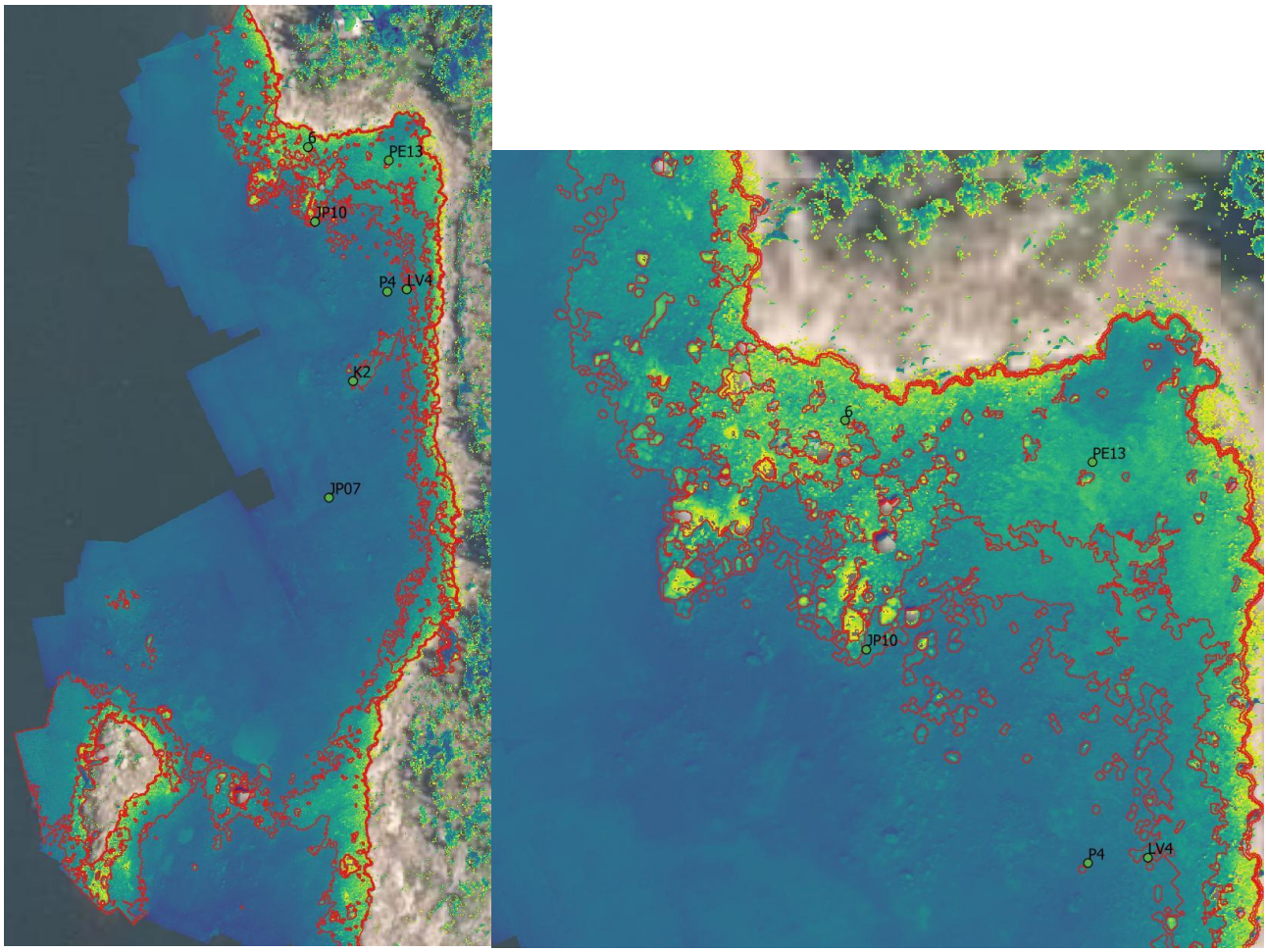

Figure 35. Example of felzenszwalb segmentation for whole Kaskinen area (left) and zoomed detail from the top of the area (right). Also, in situ sample locations are shown on both images.

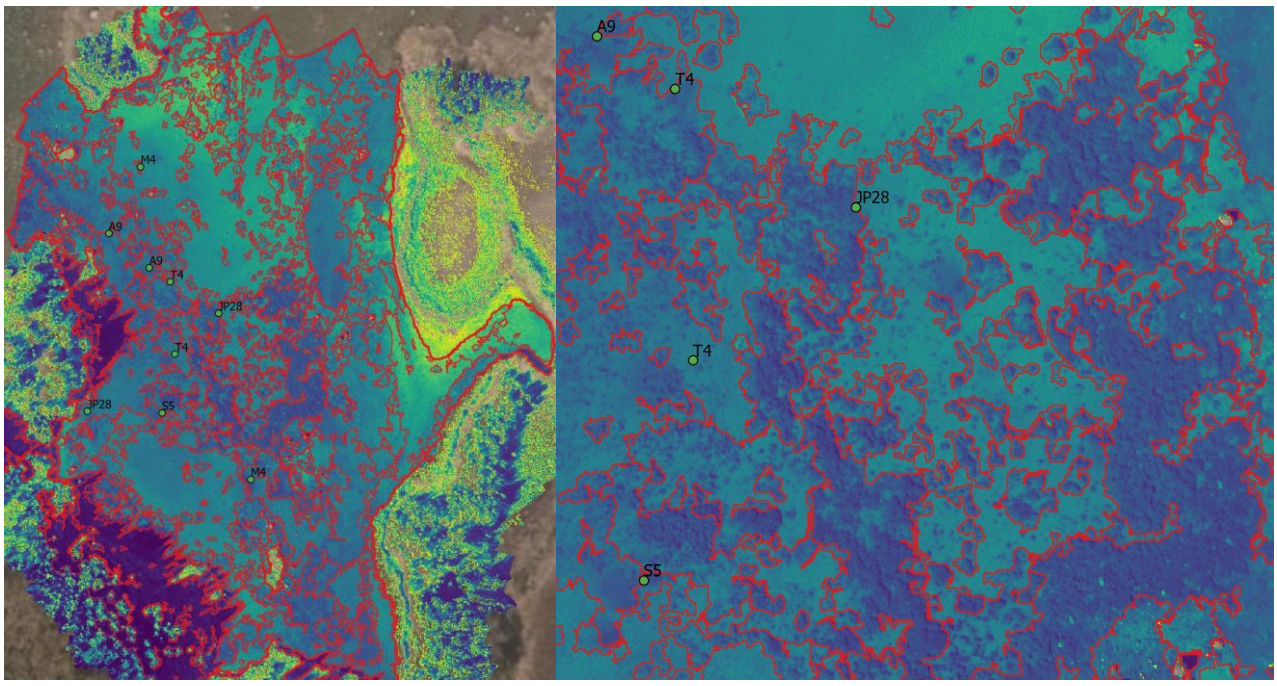

Figure 36. Example of felzenszwalb segmentation for whole Huljan area (left) and zoomed detail from the top of the area (right). Also, in situ sample locations are shown on both images.

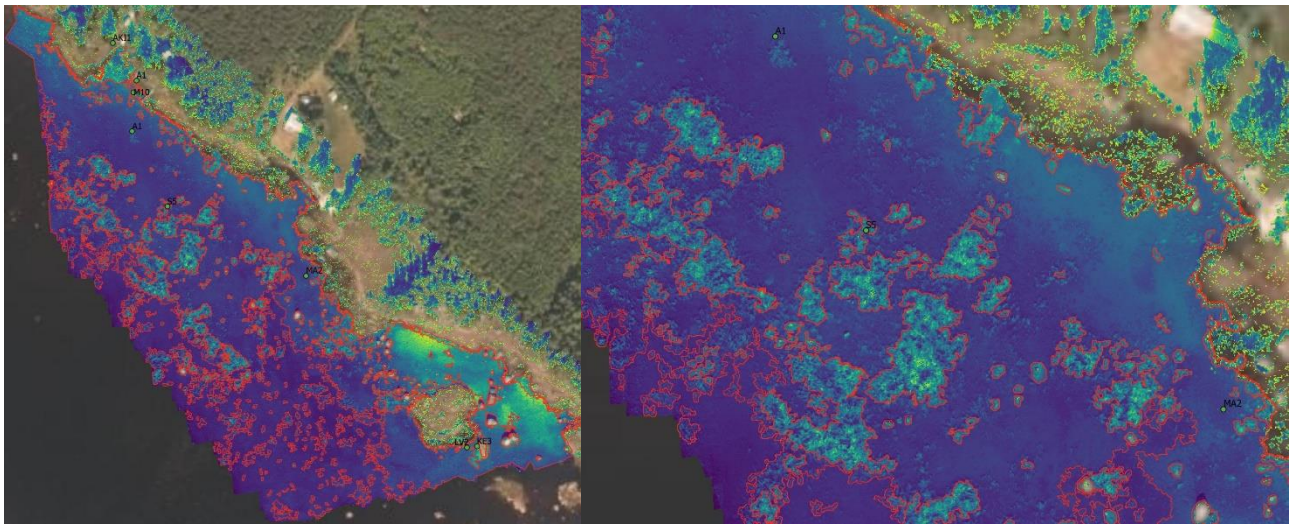

Figure 37. Example of felzenszwalb segmentation for whole Haggisgrund area (left) and zoomed detail from the top of the area (right). Also, in situ sample locations are shown on both images.

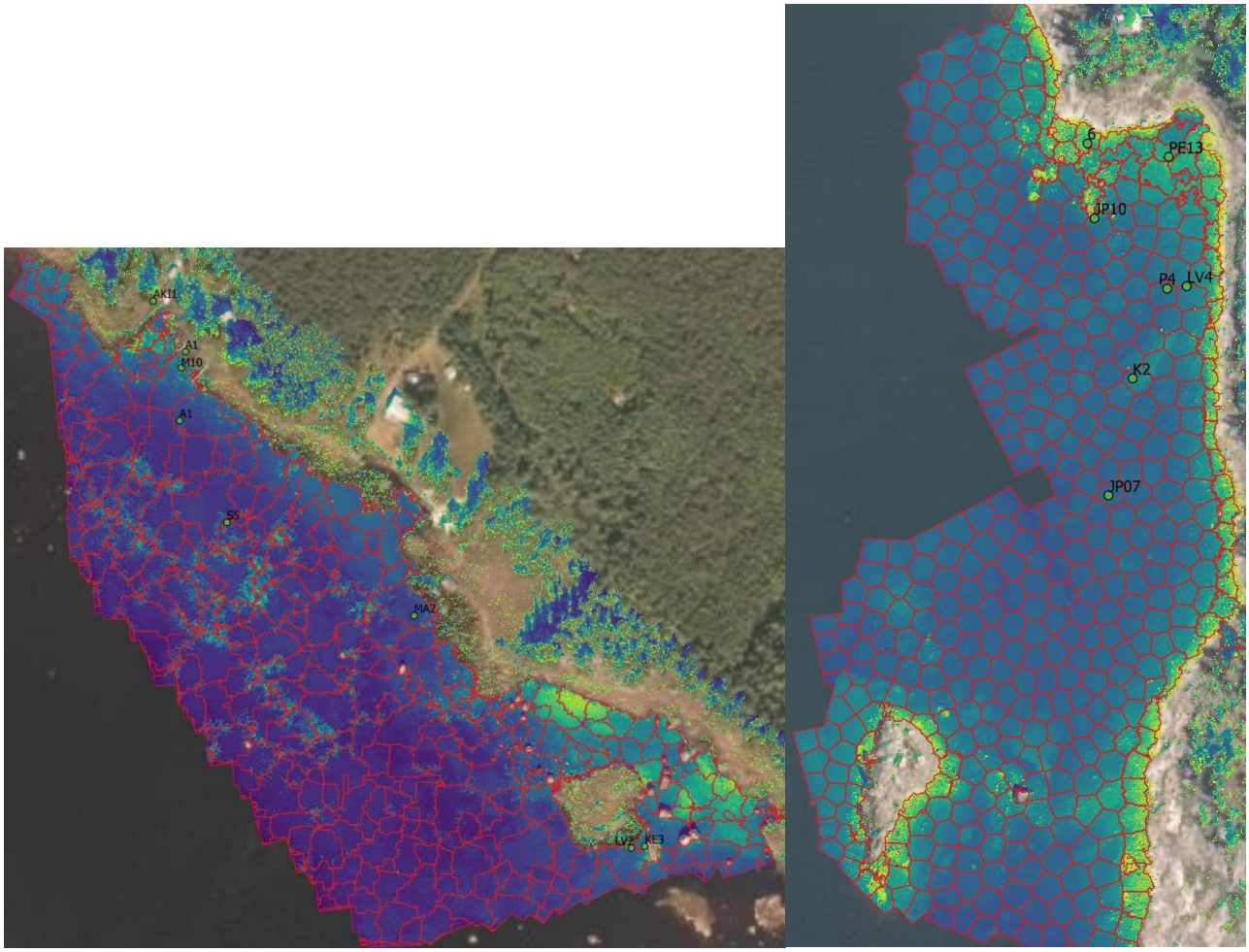

Figure 38. Left: quickshift segmentation of Haggisgrund area. Right: slic segmentation of Kaskinen area.

4.3. Discussion on challenges faced during the data analysis

Drone data processing and analysis was done as well as possible with given time and resources limitations. The challenges faced during the analysis are discussed in the following paragraphs and categorized to following themes: challenges related to sensors, challenges related to *in situ* reference spectra measurements, and challenges related to data processing and analysis.

Challenges related to sensors: FGI REHU was used as main sensor for image data collection. Snapshot imaging principle is well suited for water targets, as it collects one hyperspectral data cube (image) at single snapshot so surface waves do not interfere different bands. Dark water object sets strict requirements for image exposure: exposure time should be as long as possible to get strong signal, but short enough so that drone movement is does not blur the image. The hyperspectral imagery collected from Kaskinen was underexposed, producing sub-optimal data.

Dark water sets also strict requirements also for sensor calibration and image reflectance conversion. In this work, REHU HS imagery was converted to reflectance using three reference reflectance panels, and the accuracy of the conversion is estimated to be about 2% in reflectance units (reflectance range [0,1]). For objects under water, we obtained reflectance values in the range of [-0.01, 0.09] with REHU VIS sensor and [-0.075, 0.05] with REHU NIR sensor respectively. These values are extremely low, and especially basically all REHU NIR data values were negative, but still inside the estimated reflectance accuracy of 2%. With objects as dark as these, even small error in reflectance conversion can produce clearly visible error to reflectance spectra. Especially for NIR data, where the water absorbs strongly the light it would have been advantageous to have some reference targets on the sea bottom to make more precise calibration. During this work, we were not able to improve the accuracy of REHU NIR data and match it to be usable with REHU VIS spectra, so only images from REHU VIS sensor were used in data analysis.

Also, spectral response shape of the raw REHU HS bands are not clean Gaussian, but some bands have relatively large side peaks at different wavelength range than the main center wavelength. This adds challenges to the spectral analysis using data from REHU HS sensors.

Finally, the GPS accuracy of *in situ* samples collected by Metsähallitus was on the level of meters. This means that for small sample, the GPS location used to extract image derived spectra for this sample location might not be at correct place. This adds uncertainty to the analysis presented in this report, and we were not able to verify that image derived *in situ* spectra were really of the correct species.

Challenges related to *in situ* reference spectra measurements: Many sample species had complex structure with leaves and branches. Acquiring single reliable, representative spectra of each sample is highly challenging or even impossible. We performed in situ spectral measurements of samples following best known practices, acquired multiple individual spectra from each sample and averaged them to get as representative single spectra per sample as possible. Still it is difficult to estimate the quality of the reference spectra used. Also, the samples were measured on land, and many species have different shape in water as they float more freely. This adds uncertainty to comparison between in situ reference spectra and image derived spectra.

Unfortunately, there were no *in situ* samples of *Ranunculus* species or any *Hippuris* species, so it was not possible to analyze spectra of these species. Also, we were not able to study research question related to epiphytic algae and its effect to spectrum of Fucus, as it would have needed a biologist to explain and show what epiphytic algae is.

Challenges related to data processing and analysis: We were able to calculate DTMs and DSMs of each area, but we were not able to correct them from water refraction. This means that the water depth and subsurface vegetation height values have some errors. Also, we were not able to use the water depth information to correct wavelength dependent effect to object reflectance spectra. This means that the image derived spectra have higher errors on longer wavelengths i.e. on red and NIR

range. These errors in image derived spectra adds challenges to spectral angle mapper classification when comparing image derived and *in situ* reference spectra.

We were able to perform image segmentation to find areas of different species, but we were not able to verify the quality and accuracy of the image segments. All tested segmentation algorithms would require more iterative work and expert knowledge to get reliable results. Also, due to time limitations, we were not able to test classifying the image segments with respect to *in situ* reference data.

It seems that the simple DTM extraction method of Metashape was not performing very accurately in the noisy areas e.g. in the center of the Huljan bay. In visual inspection, the less processed DSM indicates the water depths to be of approximately 90 cm, while the DTM shows depths of 120-150 cm at the bottom of the noisy point cloud. This indicates that the processes for filtering noise and extraction of the DTM should be improved if reliable data is needed for depths beyond 60 cm.

5. Conclusions and future work

The results achieved in this project showed that hyperspectral imaging from drone is suitable and promising method for mapping shallow water habitats. We were able to create digital terrain models (DTM) of shallow sea bottom up to 1 meter depth and digital surface models (DSM) describing the height of the sea floor habitats by using RGB images and standard photogrammetric processing workflows. We collected *in situ* spectral library of species samples and evaluated the possibilities to separate different species based on their spectra. We used spectral angle mapper for pixel-based classification of image mosaics to classes defined by *in situ* reference spectra. We were able to create spectral angle maps showing potential areas for selected sample species. We performed segmentation of hyperspectral image mosaics using three different algorithms. These segmentation results can illustrate the potential vegetation areas and patch sizes of different species.

Results obtained in this work are indicative regarding the potential of drone-based hyperspectral imaging for shallow water habitat mapping. There are several topics for further studies and potential ways to improve research results. These topics are discussed in the following and categorized to following themes: sensor and image collection related work, in situ reference measurements, and data processing and analysis.

Sensor and image collection related work: in the future hyperspectral drone campaigns over water areas, the sensor exposure setting values should be set carefully to collect as strong signal as possible without adding any disturbances from the platform movement. It would be also possible to collect images over specific targets in still, hovering mode i.e. to stop over area of interest.

Sensor calibration and image reflectance transformation should be performed as accurately as possible, as dark water target sets strict requirements for reflectance accuracy. We should improve the accuracy of REHU NIR sensor data and evaluate the usefulness of information collected in the NIR spectral range. Due to water absorption it is evident that less information is gathered of the object at longer wavelengths, but there could be still some additional information that could help the image segmentation and classification accuracies. We should evaluate the signal-to-noise -ratio (SNR) of the REHU HS sensors over dark targets to see how much useful signal we can get over water.

In this study, we used raw REHU HS bands for data analysis. As many of the bands have high side peaks at different wavelength range than the band main center wavelength, spectral analysis of the data is challenging. We should evaluate possibilities to mathematically calculate gaussian-shaped REHU HS virtual bands that would be optimized for dark water targets. There already exists REHU HS virtual bands suitable for land applications, but they were not usable in this work.

Ground sampling distance (GSD) of the collected images is always tradeoff between the high spatial accuracy and large area coverage i.e. we get better GSD from lower flying altitude, but the covered

area is then smaller. More work should be done on finding the optimal GSD for separating different bottom habitats and their patch sizes.

Work related to in situ measurements: It would be good to collect comprehensive spectral library of various *in situ* samples. Library should include several spectra of the same species to illustrate the within species variance. Also, each species should be measured during different times of the growing season, and optimally measurements should be done in sample's natural environment in the water. This kind of spectral library could be used to train machine learning and deep learning classification algorithms.

When comparing differences and similarities between *in situ* reference spectra, spectral angle and Chi-square metrics could be calculated only to reduced wavelength range such as 400 - 600 nm, compared to full 400 – 1000 nm range used in this work. Usage of reduced spectral range would highlight the differences or similarities of sample spectra in the most important spectral range on water applications.

Work related to data processing and analysis: Water depth values on DTMs and DSMs should be corrected for water refraction to get accurate water depth and vegetation height values. Easiest way for this correction would be to use reference depth measurements from the area of interest. Accurate DSM and DTM should be then used for performing wavelength dependent water absorption correction for image derived spectra. This would improve especially the quality of the information collected on longer wavelengths in the red and NIR spectral ranges. There are several empirical, semi-empirical and physical correction methods for water absorption. These were shortly discussed in the preliminary project report (Markelin 2020).

Image analysis should be performed only for the area of interest, and unnecessary areas such as land should be masked out. By utilizing DSM/DTM information in combination with spectral data, it should be possible to create more accurate and better masks for water areas.

More effort should be put on the creation of realistic and accurate segmentation of hyperspectral image mosaics. Segmentation should describe the spatial extent and patch sizes of species accurately with realistic number of segments.

Finally, there are several ways for improving the image classification. One way to overcome the spectral differences between *in situ* reference spectra measured on land and image derived spectra of samples in water would be to use actual image derived spectra from sample locations as reference data for classifying whole image area. This would already improve the results of the relatively simple spectral angle mapper -classification used in this work. Then, confidence intervals of reference spectra could be utilized in the classification, and confidence estimates for classification results could be calculated. This would give uncertainty estimation for each class. The classification should also give probabilities of each reference to certain pixel/segment. Finally, to achieve more accurate results, the image classification should utilize not only spectral features, but combine spectral, textural and 3D features. There are several commercial and open source software packages, which include multiple different machine learning algorithms that could be evaluated for hyperspectral image segmentation and classification, such as eCognition (https://geospatial.trimble.com/products-and-solutions/ecognition), ENVI (https://www.l3harrisgeospatial.com/Software-Technology/ENVI, RSGISLib (https://rsgislib.org/), QGIS etc.

6. List of references

Adapthist 2021. Scikit-image processing, module exposure, documents for version 0.18.0. Contrast Limited Adaptive Histogram Equalization (CLAHE) algorithm. Accessed 31.5.2021. https://scikit-image.org/docs/0.18.x/api/skimage.exposure.html?highlight=equalize_adapthist#skimage.exposure.equalize_adapthist

Honkavaara, E., Khoramshahi, E., **2018**. Radiometric Correction of Close-Range Spectral Image Blocks Captured Using an Unmanned Aerial Vehicle with a Radiometric Block Adjustment. Remote Sensing 2018, 10, 256. DOI: https://doi.org/10.3390/rs10020256

Kruse, F.A., Lefkoff, A.B., Boardman, J.W., Heidebrecht, K.B., Shapiro, A.T., Barloon, P.J., Goetz, A.F.H. 1993. The spectral image processing system (SIPS)—Interactive visualization and analysis of imaging spectrometer data. Remote Sensing of the Environment. 1993, 44, 145–163. DOI: https://doi.org/10.1016/0034-4257(93)90013-N

Markelin, L., Simis, S.G.H., Hunter, P.D., Spyrakos, E., Tyler, A.N., Clewley, D., Groom, S. **2017**. Atmospheric Correction Performance of Hyperspectral Airborne Imagery over a Small Eutrophic Lake under Changing Cloud Cover. Remote Sensing 2017, 9, 2. DOI: https://doi.org/10.3390/rs9010002

Markelin, L. 2020. Preliminary survey: literature review of shallow water marine habitat mapping with drones, and plans for drone imaging and field sampling at Vaasa. Delivered to Metsähallitus on 28 August 2020.

Nevalainen, O., Honkavaara, E., Tuominen, S., Viljanen, N., Hakala, T., Yu, X., Hyyppä, J., Saari, H.; Pölönen, I., Imai, N.N., Tommaselli, A.M.G. **2017**. Individual tree detection and classification with UAV-based photogrammetric point clouds and hyperspectral imaging. Remote Sensing, 2017, 9, 185. DOI: https://doi.org/10.3390/rs9030185

Smith, G.M. & Milton, E.J. **1999**. The use of the empirical line method to calibrate remotely sensed data to reflectance, International Journal of Remote Sensing, 20:13, 2653-2662, DOI: https://doi.org/10.1080/014311699211994

Suomalainen, J., Hakala, T., de Oliveira, R.A., Markelin, L., Viljanen, N., Näsi, R., Honkavaara, E. **2018** A Novel Tilt Correction Technique for Irradiance Sensors and Spectrometers On-Board Unmanned Aerial Vehicles. Remote Sensing, 2018, 10(12), 2068. DOI: https://doi.org/10.3390/rs10122068

Skimage 2021. Scikit-image processing, module segmentation, documents for version 0.18.0. Accessed 31.5.2021. https://scikit-image.org/docs/0.18.x/api/skimage.segmentation.html

SpectralPython 2021. Spectral Python 0.21 documentation, Spectral Python (SPy) User Guide. Accessed 31.5.2021. https://www.spectralpython.net/class_func_ref.html#spectral.algorithms.algorithms.msam